Proximal termination generates a transcriptional state that determines the rate of establishment of Polycomb silencing

Govind Menon[1,†], Eduardo Mateo-Bonmati[2,5,†], Svenja Reeck[2], Robert Maple[2], Zhe Wu[3], Robert Ietswaart[4], Caroline Dean[2,*], Martin Howard[1,*]

[1]Department of Computational and Systems Biology, John Innes Centre, Norwich Research Park NR4 7UH, UK

[2]Department of Cell and Developmental Biology, John Innes Centre, Norwich Research Park NR4 7UH, UK

[3]Key Laboratory of Molecular Design for Plant Cell Factory of Guangdong Higher Education Institutes, Institute of Plant and Food Science, Department of Biology, School of Life Sciences, Southern University of Science and Technology, Shenzhen, China

[4]Harvard Medical School, Department of Genetics, 77 Avenue Louis Pasteur, Boston, MA 02115, USA

[5]Current address: Centro de Biotecnología y Genómica de Plantas, Universidad Politécnica de Madrid (UPM) – Instituto Nacional de Investigación y Tecnología Agraria y Alimentaria (INIA)/CSIC, 28223 Pozuelo de Alarcón, Madrid, Spain

[†]These authors contributed equally to this work

[*]Co-corresponding authors: caroline.dean@jic.ac.uk, martin.howard@jic.ac.uk

Abstract

Chromatin-mediated transcriptional states are central to gene regulation in development and environmental response, with co-transcriptional processes involved in their establishment. Quantitative regulation of Arabidopsis *FLOWERING LOCUS C* (*FLC*) is key to determining reproductive strategy. Low *FLC* expression underpins rapid-cycling and is established through a transcription-coupled chromatin mechanism. Proximal termination of antisense transcripts is linked to histone 3 lysine 4 demethylation of adjacent chromatin that leads to stable Polycomb Repressive Complex 2 (PRC2) silencing. However, how the termination-induced chromatin environment influences the switch to PRC2 silencing is still unclear. Here, we combine molecular approaches with theory to develop a dynamic mathematical model that incorporates sense/antisense transcription, alternative termination sites, and the interplay of these processes with varying levels of activating (H3K4me1)/silencing (H3K27me3) histone modifications. The model captures different feedback

mechanisms between co-transcriptional 3' processing and chromatin modifications, detailing how proximal co-transcriptional polyadenylation/termination can set the subsequent level of productive transcription via removal of H3K4 monomethylation across the locus. Since transcription universally antagonizes Polycomb silencing, this dictates the degree of antagonism to H3K27me3, thus determining the rate at which Polycomb repression is established. These principles are likely to be central to regulating transcriptional output at many targets and generally relevant for Polycomb silencing in many genomes.

Introduction

Transcriptional regulation is often mediated by chromatin states that are key to developmental changes and environmental responses in many organisms. These chromatin states are characterised by histone modifications, and trans-factors that recognise these modifications, which together determine the level of productive transcription. Such chromatin states can be heritable across DNA replication and mitosis, with controlled switching of key developmental loci between active and silenced states underpinning the changes in gene expression programs that drive differentiation.

These inheritance mechanisms include read-write reinforcement of existing histone modifications and antagonism between transcription and repressive modifications (Berry et al., 2017; Dodd et al., 2007; Holoch et al., 2021). Such mechanisms can be bistable producing all or nothing (ON or OFF) transcriptional activity (Berry et al., 2017; Pease et al., 2021). Each gene copy can be stably maintained in either an ON or OFF state even in dividing cells and can be autonomously switched between states. The population level gene expression is then determined by the fraction of copies in the ON state (Alamos et al., 2021; Antoniou-Kourounioti et al., 2023; Berry et al., 2015; Ng et al., 2018; Saxton and Rine, 2022; Siwek et al., 2020).

We have studied this mode of regulation at the Arabidopsis floral repressor gene *FLOWERING LOCUS C* (*FLC*). Most well-known is the winter-induced silencing of *FLC* by PRC2. The winter cold-induced epigenetic silencing is an ON/OFF cell-autonomous, stochastic switching of individual *FLC* copies into a Polycomb silenced state (Fig. 1A) (Angel et al., 2011; Berry et al., 2015; Csorba et al., 2014; Lövkvist and Howard, 2021; Menon et al., 2021). In this process, the silencing histone modification H3K27me3 is deposited at a specific intragenic site during the cold, followed by spreading of H3K27me3 across the locus through a cell-cycle dependent mechanism during growth after cold.

Fundamentally different to the *cis*-mediated ON/OFF mode is regulation of gene expression in a graded manner (Fig. 1A). Such a graded level can be set by the concentration (Giorgetti et al., 2010; Lammers et al., 2020) or activation strength of transcription factors (Mamrak et al., 2022),

conceptually similar to how a dimmer can control the intensity of a light. These analogue mechanisms mainly function in *trans*, with approximately uniform expression at each gene copy. This type of analogue mechanism also occurs at *FLC* to set the quantitative expression level that determines reproductive strategy. Low expression is established in a mechanism involving the RNA binding protein FCA, which promotes proximal termination of *FLC* sense transcription in the developing embryo (Schon et al., 2021), and of antisense transcription in the seedling (Liu et al., 2010). Also essential is FLD, a plant homologue of the conserved histone K4 demethylase LSD1 (Martignago et al., 2019). Utilising an allelic series for *fca*, together with quantitative imaging, we showed that this FCA-regulated, transcription-coupled mechanism can generate a graded, analogue regulation of *FLC* expression (Antoniou-Kourounioti et al., 2023).

This analogue mechanism is a prelude for a PRC2-dependent digital ON/OFF expression switch that occurs at different frequencies in different *fca* alleles (Fig. 1B) (Antoniou-Kourounioti et al., 2023). The key question we therefore set out to answer in the work described here is how factors that mediate the *analogue* mode of *FLC* regulation (3' co-transcriptional processing machinery linked to histone H3K4 demethylation (Fang et al., 2020)) feed into the Polycomb ON/OFF *digital* mode of regulation. Such transcription-coupled mechanisms have been implicated in the establishment of chromatin states in many organisms, through 3' processing and non-coding RNA. A recent study indicates a wide-ranging role for 3' processing in heterochromatin establishment in *S. pombe* (Shimada et al., 2021). For example, Clr4-mediated heterochromatin assembly by the RNAi-independent pathway involves non-canonical polyadenylation and 3' processing factors (Chalamcharla et al., 2015; Tucker et al., 2016; Vo et al., 2019). Transcription termination at non-canonical sites mediated by the conserved cleavage and polyadenylation factor (CPF) and the RNA-binding protein Mmi1 have been shown to be necessary for Clr4-driven assembly of facultative heterochromatin at meiotic and environmental response genes. Another RNA binding protein, Seb1, has been shown to promote heterochromatin formation, through a mechanism linked to termination of noncoding transcription (Marina et al., 2013; Wittmann et al., 2017). Nevertheless, the exact mechanisms linking RNA termination/processing and chromatin regulation are still poorly understood.

Here, using mathematical modelling combined with molecular approaches, we elucidate the interactions between co-transcriptional processing and chromatin regulation that underpin transcription-coupled repression leading to Polycomb-mediated low expression of *FLC*. Specifically, the model describes sense and antisense transcription, alternative transcriptional termination, the dynamics of activating (H3K4me1) and silencing (H3K27me) modifications, and the interactions between these components (Fig. 1C, D). We constrained the model using existing experimental data and showed that it can successfully generate intermediate transcriptional outputs at non-Polycomb

silenced *FLC* copies (analogue regulation), while also allowing Polycomb nucleation to occur slowly over time (digital switch). We then used the model to predict changes in activating H3K4me1 and silencing H3K27me3 modifications at *FLC* over time and validated these predictions over a developmental time-course. The model clearly elaborates the steps and feedbacks in how FCA/FLD-mediated transcription-coupled repression, induced by co-transcriptional processing steps, described in the accompanying paper (Mateo-Bonmatí et al., 2023), influence the timing of the digital switch to Polycomb silencing. The combination of molecular genetics and the theoretical modelling described here provide a quantitative description of how co-transcriptional processing sets transcriptional states that determine rates of Polycomb silencing, a mechanism that is likely to be generally relevant in many organisms.

Results

Molecular network governing the *FLC* transcription-coupled chromatin repression pathway

The RNA binding protein FCA promotes proximal polyadenylation/termination at many targets in the Arabidopsis genome (Sonmez et al., 2011). FCA is known to directly interact *in vivo* with FY, a CPSF component needed for silencing homologous to yeast Pfs2 and mammalian WDR33 (Simpson et al., 2003). FCA also indirectly interacts with other cleavage and polyadenylation specificity factors (Fang et al., 2019), as well as the 3' processing factors CstF64 and CstF77 (Liu et al., 2010). FCA-mediated silencing also requires the involvement of CDKC2, a component of the transcription elongation factor P-TEFb (Wang et al., 2014), as well as the core spliceosome component PRP8 (Marquardt et al., 2014), suggesting it is the process of transcription and proximal termination, rather than just the transcripts themselves, that drive silencing.

The fate of the proximally polyadenylated transcripts is different dependent on which strand is being transcribed. The *FLC* sense proximal transcripts are detectable in young embryos (Schon et al., 2021) but less so in vegetative tissue, likely due to rapid nascent RNA turnover. In contrast, the *FLC* antisense RNAs transcribed from the 3' end of *FLC* (collectively called *COOLAIR*), which are alternatively polyadenylated (PA) at a proximal PA site within the *FLC* gene or a distal PA site in the vicinity of the *FLC* promoter (Liu et al., 2010; Swiezewski et al., 2009), are both relatively stable. The mechanism underlying the differential turnover of proximally polyadenylated transcripts is currently unknown, but differential fates of coding and non-coding transcripts are not uncommon (Nojima and Proudfoot, 2022).

To further test the antisense transcript role we examined *FLC* repression in an FCA overexpression line, comparing expression of a wild-type *FLC* transgene (*FLC-15*), with that of an *FLC* transgene

where the antisense promoter has been replaced - *TEX 1.0* (Csorba et al., 2014). The *FLC* repression observed for the wild-type *FLC* transgene is significantly attenuated ~10 fold in *TEX 1.0*, supporting a role for antisense transcription in FCA-mediated silencing (Fig. 2A). Similar results were found using a CRISPR deletion of the antisense promoter at the endogenous *FLC* locus (Zhao et al., 2021). The remaining repression of *FLC* silencing by the defective antisense lines raised the question of the importance of FCA-mediated proximal termination of *FLC* sense transcription. We therefore analysed production of sense polyadenylated *FLC* transcripts by Quant-seq (Moll et al., 2014). Proximally polyadenylated transcripts for the *FLC* transcript were detected for all genotypes analysed (Fig. 2B), although levels were very low, potentially due to differential fates of coding/non-coding transcripts described above. The sites of proximal termination in seedlings were similar to those reported in embryos (Schon et al., 2021). Altogether these data support a model whereby FCA-mediated proximal termination of both sense and antisense transcription contributes to repression of *FLC* transcription.

FLC silencing mediated by FCA requires the protein FLD, a homologue of the mammalian H3K4/K9 demethylase LSD1 (Liu et al., 2007). FLD is thought to demethylate H3K4me1 in Arabidopsis (Inagaki et al., 2021; Martignago et al., 2019). FLD has been shown to associate in vivo with the SET domain protein SDG26, which interacts with FY, indicating a physical link between processing of antisense transcripts and chromatin remodelling (Fang et al., 2020). FLD also stoichiometrically associates in vivo with LD, a TFII-S domain containing protein and homolog of the CPSF phosphatase subunit, PNUTS in human and Ref2 in yeast. This strong association of chromatin remodelers such as FLD with RNA Pol II regulators shown in the accompanying paper, identifies a mechanism where FCA-mediated proximal cleavage and polyadenylation triggers FLD-mediated removal of H3K4me1 (Mateo-Bonmatí et al., 2023). Removal of H3K4me1 then further affects co-transcriptional splicing of sense and antisense transcription, potentially via reduced H3K36me3, whose methyltransferase SDG8 recognises H3K4me1. This could in turn promote further early transcription termination in a feedback loop.

What determines the polyadenylation site choice? At *FLC*, this has been easiest to address via *COOLAIR* processing, given the likely rapid turnover of sense proximally polyadenylated transcripts. FCA is proposed to recognize any situation where RNA Pol II has stalled and transcription termination is required to clear a ‘tangle’ in the chromatin prior to replication (Baxter et al., 2021; Xu et al., 2021). The above molecular mechanisms and possible feedback interaction are summarised in the schematic shown in Fig. 1C.

Computational model of *FLC* chromatin silencing through alternative termination

The stable silenced state of *FLC* eventually generated by this co-transcriptional repression mechanism is a Polycomb silenced state, with the locus covered by H3K27me3 (Wu et al., 2016). This is

consistent with genetic analysis indicating that the plant Polycomb methyltransferase CURLY LEAF (CLF) is essential for FCA-mediated silencing of *FLC* (Fang et al., 2020). However, despite the detailed molecular data on 3' processing-mediated silencing described above, and in the accompanying paper (Mateo-Bonmatí et al., 2023), it remains unclear how the various elements fit together to generate a transition into Polycomb silencing. To bridge this gap, we therefore constructed a computational model based on the above features (Fig. 1D). We then combined this model with our prior knowledge of Polycomb dynamics, which is known to generate digital ON/OFF memory states (Fig. 3A). We then used this model to dissect the underlying mechanism of the transition elucidating how such digital silencing might be integrated into FCA-mediated 3' processing. Note that our previous model (Wu et al., 2016) also analysed transcription of the repressed state, which revealed reduced initiation and slower elongation; however, it did not address the mechanism of switching into silencing. Important features of the new model are described below:

The model includes both activating and repressive histone modifications across the *FLC* locus, specifically activating H3K4me1 and repressive H3K27me2/me3, which are mutually exclusive on the same H3 tail. The model also incorporates sense and antisense transcription events at the locus, where the frequency for both (representing either transcription initiation or transition to elongation) is determined by the overall coverage of repressive H3K27me3. Activating H3K4me1 modifications are added co-transcriptionally, with higher overall coverage of H3K4me1 across the locus promoting distal termination of transcription (as proposed above). Proximal termination of both sense and antisense transcription can then mediate removal of H3K4me1, in line with the potential function of FLD as a demethylase. The model also describes deposition of H3K27me by Polycomb in the *FLC* nucleation region. H3K27me spreads to the rest of the locus through interactions with the nucleation region, through well-characterised read-write feedback interactions. Experimental evidence indicates the existence of a gene loop mediating an interaction between the 5' and 3' ends of *FLC:* this interaction is also captured in the model. Finally, in line with experimental evidence from mammalian systems and previously developed models for Polycomb, the model assumes that productive transcription promotes removal of H3K27me through both histone exchange and co-transcriptional demethylation. Full details of the model can be found in the Methods and Supporting Information.

Quantitative modulation of transcriptional output influences the timing of the digital ON/OFF Polycomb switch

We have previously experimentally analysed *FLC* expression using an allelic series of *fca* mutants (Antoniou-Kourounioti et al., 2023; Koornneef et al., 1991). These mutants show a range of *FLC* expression (assayed through a Col-0 *FLC*-Venus transgene) at the whole plant level, ranging from low in the parental Landsberg *erecta* (L*er*) genotype, through higher expression levels in an

intermediate *fca-3* mutant, to a null *fca-1* mutant with the highest *FLC* expression (Antoniou-Kourounioti et al., 2023). Expression at the single cell level in root meristematic cells had been measured both by quantification of *FLC* mRNA using single molecule fluorescence *in situ* hybridization (smFISH) and of FLC protein by confocal imaging of Venus tagged FLC (Antoniou-Kourounioti et al., 2023). This analysis highlighted that the differences in overall expression between the three genotypes appeared to have two components – a digital ON/OFF mode where we observed clear differences in the number of *FLC* OFF cells, and an analogue mode, with quantitatively different levels of *FLC* in the ON cells, where, for example, *fca-3* ON cells express less than *fca-1* ON cells (Fig. 1B). The intermediate expression level in *fca-3*, was associated with a slower switch off over time into the digital OFF state. Importantly, we also observed similar behaviour of *FLC* expression in single cells for a different intermediate mutant of *FCA*, called *fca-4* (Fig. S5 and (Antoniou-Kourounioti et al., 2023)), showing effects were not allele-specific, but related to the regulatory function of FCA at *FLC*. Overall, this demonstrates that FCA quantitatively modulates transcription to influence the timing of the Polycomb switch.

We first tried to see if the model could capture the quantitative variation in *FLC* expression (analogue mode) in the absence of the Polycomb module (see model schematic in Fig. 1D). To represent the difference in FCA function between the three genotypes, we used a single parameter controlling the probability of FCA mediated proximal termination of transcription. We then simulated the model with different values for this parameter representing different levels of functionality of the FCA protein. We set the parameter to its highest value for L*er*, an intermediate value for *fca-3*, and lowest for *fca-1* (Fig. 3B). With these parameter settings we found that the model, with just transcription-coupled repression (Fig. 1D) was able to recapitulate the analogue mode of regulation, with the simulations showing the lowest frequency of productive transcription events for L*er*, highest for *fca-1*, and intermediate for *fca-3* (Fig. 3C). Consistent with the relationship between productive transcription and H3K4me1 in the model, the levels of this modification were also predicted to be lowest in L*er*, intermediate in *fca-3* and highest in *fca-1* (Fig. 3D). Then, keeping all other parameters fixed, we adjusted the values of the FCA effectiveness parameter so that the ratios of productive transcription frequencies at steady-state matched the ratios of mean transcript levels observed by smFISH for the three genotypes (Antoniou-Kourounioti et al., 2023).

With the analogue module further constrained in this way, we simulated the full model, including the Polycomb digital switching module (Fig. 3A). Importantly, this model recapitulated the experimentally observed (Antoniou-Kourounioti et al., 2023) reduction in *FLC* transcriptional output (Fig. 3E), as well as the digital switch to stable silencing (one-way switch) over time (Fig. 3F) observed using *FLC*-Venus imaging in root meristematic cells (Antoniou-Kourounioti et al., 2023). For L*er*, where productive transcription is lowest, the model predicted a rapid switch to the digital

OFF/Polycomb silenced state (Fig. 3E). For *fca-3*, the model predicted a much slower switch, with very infrequent switching for *fca-1* (Fig. 3F, S4A,B). In all cases, the switching was predicted be one-way, with the Polycomb silenced state being highly stable.

Thus, the combined model of transcription-coupled repression and Polycomb silencing predicts that the level of productive transcriptional activity set by the FCA/co-transcriptional silencing/FLD (analogue) module determines the level of transcriptional antagonism to H3K27me3. The level of antagonism in turn dictates the rate of switching to the Polycomb silenced state.

Chromatin states in different genotypes can be predicted

We next used the combined model to predict population levels of H3K4me1 and H3K27me3 at *FLC* in the three genotypes, predicting low H3K4me1 and high H3K27me3 levels in L*er*, intermediate levels of both modifications in *fca-3*, and high H3K4me1 and low H3K27me3 in *fca-1*. Starting from an active chromatin state with full H3K4me1 coverage, the model also predicted a progressive reduction in H3K4me1 over time in both L*er* and *fca-3*, while it reaches a relatively high steady-state level in *fca-1*. In L*er* and *fca-3*, this reduction is combined with an accumulation of H3K27me3 as more loci switch to the Polycomb silenced state (Fig. 4A,B).

To validate these predictions, we performed a time course measurement of H3K4me1 and H3K27me3 over the locus by chromatin Immunoprecipitation followed by quantitative PCR (ChIP-qPCR), examining their levels in seedlings at 7, 14 and 21 days after sowing. Consistent with model predictions, at all timepoints we see that *fca-3* has intermediate levels of H3K4me1 and H3K27me3, while L*er* always has the lowest H3K4me1 levels and highest H3K27me3 levels, and *fca-1* the highest H3K4me1 and lowest H3K27me3 levels. The changes in histone modifications over time are also overall qualitatively consistent with the model, with H3K27me3 levels rising and H3K4me1 levels falling over time (Model predictions: Fig.4A-C; Experimental measurements: Fig. 4D-H), as more loci switch in the digital OFF state. In L*er*, H3K4me1 shows essentially no change over the experimental timepoints, while the H3K27me3 level clearly increases in this genotype. The model predicts faster dynamics of the transcription coupled repression (relative to slow Polycomb silencing establishment): this is seen in the predicted histone modification dynamics in L*er* and *fca-3*, where during the initial phase (0 to 7 days) the H3K4me1 levels clearly reduce faster than the rate of H3K27me3 accumulation. The lack of change in experimentally measured H3K4me1 is therefore consistent with the model prediction: by the 7-day timepoint, H3K4me1 may already be maintained at a low level by the FCA/FLD mediated repression or nucleation of Polycomb, so that subsequent H3K27me3 accumulation has little effect on these levels. We note that this lack of reduction is consistent with the observed increase in H3K27me3 mainly resulting from spreading of this mark

across the locus: H3K4me1 exhibits similar behaviour during post cold growth, showing very little change during a phase where H3K27me3 spreads across the locus (Nielsen et al., 2023). The activating H3K36me3 also shows a similar pattern, with *fca-3* exhibiting intermediate levels, and the overall levels decreasing over time (Fig. S4C,D). The predicted differences in the ratio of proximal to distal polyadenylation of sense transcripts between the *FCA* mutants and the parental genotype also qualitatively matched the measured ratios for *FLC* sense transcription in our Quant-seq dataset (Fig. 4C,F).

Overall, the combined model of transcription-coupled repression, mediated by proximal termination of transcription, and Polycomb silencing, successfully predicts both the relative levels of the modifications between genotypes and how these change over time.

Analogue differences are persistent but the switch to the OFF state is compromised by disrupting a Polycomb methyltransferase

The model predicts that analogue repression removes the antagonism of transcription on Polycomb and thus permits the switch to Polycomb digital silencing. We tested this model prediction further using a Polycomb mutant – a loss of function mutant of *CLF*, one of the three Arabidopsis H3K27 methyltransferases. This methyltransferase is known to be required for spreading of H3K27me3 from Polycomb nucleation peaks at many Arabidopsis targets (Shu et al., 2019), and specifically at *FLC*, both in developmental (Shu et al., 2019) and cold induced silencing contexts (Yang et al., 2017). We would not expect this mutant to completely disrupt the ON/OFF silencing mode, as H3K27me3 nucleation alone, which still occurs in *clf*, gives a metastable Polycomb silenced state (Yang et al., 2017). However, we would expect the switch to the OFF state to be partially compromised (Fig. 5A). Only after the H3K27me3 spreads across the whole locus is the Polycomb state fully stable in rapidly dividing cells (Yang et al., 2017). In the *clf* case, the model predicts that the analogue differences persist due to leakage out of the metastable Polycomb OFF state. As a result, the continued slow reduction in overall *FLC* expression – which is a consequence of a fully stable Polycomb digital switch – is predicted to be missing (Fig. 5B).

To validate this prediction, we measured *FLC* expression at the whole plant level, over a time course in five different genotypes: the parental L*er*, *clf-2* (Goodrich et al., 1997), *fca-3*, the *fca-3 clf-2* double mutant, and *fca-1*. Consistent with model predictions in the *clf* mutants, we observe that the analogue differences are maintained, but the slow reduction in expression is compromised (Fig. 5C). In addition to *FLC* expression at the whole plant level, we also conducted time course imaging of Venus tagged FLC in the roots in the *clf* mutants (Fig. 5D), following the same approach used to analyse the *fca* alleles in (Antoniou-Kourounioti et al., 2023). Again, as predicted, *clf-2* showed clear differences to

the L*er* genotype, with ON cells being visible at all three timepoints. This is consistent with *FLC* switching both ON to OFF and OFF to ON as described above, and the observed lack of reduction in *FLC* expression at the whole plant level (Fig. 5C). We note that both *clf-2* and *fca-3 clf-2* exhibited large variability between roots, with some roots showing essentially no *FLC* ON cells (Fig. S5). This is possibly due to the widespread misregulation of growth and developmental genes resulting from the compromised Polycomb silencing in this mutant. Nevertheless, consistent with the model predictions, we see that the slow Polycomb digital switch to OFF is disrupted in *fca-3 clf-2*: when comparing roots exhibiting ON cells in the double mutant to *fca-3* roots, the double mutant overall shows more ON cells at later timepoints.

The model also predicts a similar, high ratio of proximal to distal termination in the *clf* mutant and the L*er* genotype (Fig. 4C), even though overall transcription is lower in L*er*. This is because the FCA/FLD mediated transcription coupled mechanism is not disrupted in any way in the *clf* mutant model, so that the promotion of proximal termination by this mechanism, and the resulting feedback, remains intact. We measured the ratio of proximal to distal termination of the *FLC* sense transcript in the *clf* mutant, using our strand-specific Quant-seq data. Consistent with the model prediction, it exhibits a similar ratio to the L*er* genotype (Fig. 4F).

As further validation of the model, we then compared the predicted H3K27me3 levels at the locus in a *clf* mutant to experimentally measured levels. The lack of stability of the nucleated state in the model means that it predicts an H3K27me3 peak, but at significantly lower levels relative to a spread state. The incorporation of the *FLC* gene loop in the model, as outlined above, causes the model to generate a second peak in the *FLC* 3' region, in the region that interacts strongly with the nucleation region. Consistent with these predictions, we find that the ChIP profile of H3K27me3 in *clf-2* exhibits two peaks, at significantly lower levels relative to the spread state in L*er* (Fig. 5E). Our results also aligned well with previously published genome-wide H3K27me3 data for a *clf* mutant in a Col-0 background (Shu et al., 2019). Overall, predictions from the model for *clf* mutants match well with our experimental data.

Co-transcriptional occupancy of FLD at *FLC*

We next investigated the mechanism of FLD functionality in the co-transcriptional repression mechanism. In apparent contradiction to its role as a repressor, FLD occupancy was found to be significantly higher in a high transcriptional state of *FLC*, relative to a Polycomb silenced low transcriptional state. Specifically, high FLD levels were assayed by ChIP-seq of a transgenic *fld-4; 3xFLAG-FLD* in the Col*FRI* background, where the *FLC* activator FRIGIDA sets up a high

transcriptional state (Inagaki et al., 2021). In contrast, in a Col-0 background, where FRI is not functional, *FLC* is Polycomb silenced and FLD shows low enrichment.

The model allows us to explain this counter-intuitive behaviour of FLD. Since FLD function is coupled to transcription and termination in the model, it predicts that FLD targeting must be co-transcriptional, consistent with the molecular and genetic analysis in the accompanying paper (Mateo-Bonmatí et al., 2023). FLD levels at the locus must therefore be low in a Polycomb silenced state, where transcription events are infrequent. This prediction is consistent with the genome-wide correlation between FLD enrichment and transcription as measured by Pol II ChIP and transcript amounts in (Inagaki et al., 2021). Furthermore, by capturing the digital switch off in L*er* and *fca-3*, the model predicts that FLD enrichment would reduce over time in these genotypes. In essence, FLD is only needed transiently to generate a lowly-transcribed state capable of nucleating Polycomb silencing, as transcription antagonises Polycomb. Following Polycomb nucleation and spreading of H3K27me3, FLD recruitment to the locus is reduced due to the lack of transcription.

The experimental validation of the first prediction of the model (FLD coupled to transcription) is presented in the accompanying paper (Mateo-Bonmatí et al., 2023). ChIP-qPCR analysis of FLD enrichment at *FLC* in high transcription states induced by two very different genetic backgrounds (*fca-9* and *FRI*) compared with a Polycomb silenced state (Col-0) perfectly fit a co-transcriptional role for FLD. The model also supports the scenario proposed by Inagaki et al., (2021) in which FLD downregulates histone H3K4me1 in regions with convergent overlapping transcription genome-wide in Arabidopsis. Despite functioning in the same genetic pathway, FLD function, or at least localization, seems to be FCA-independent, suggesting that both activities are functionally coupled/sequential but physically disconnected.

We also tested the second model prediction that FLD enrichment would change over time as a result of the digital switch to the Polycomb silenced state. We measured 3xFLAG-FLD enrichment by ChIP-qPCR over a time course in a Col-0 background (as high-expressing *fca-9* and FRI are not expected to exhibit a digital switch OFF). Consistent with model predictions, we observed a reduction over time in FLD enrichment across *FLC* (Fig. 6B), mirroring the reduction in *FLC* transcription levels over time also observed in Col-0 by qPCR (Fig. 6A). Levels at the initial 7-day timepoint were high and declined to very low levels (almost background) by 21 days.

Together, these observations are consistent with model predictions of co-transcriptional FLD targeting to the *FLC* locus, with its repressive activity dependent on FCA-mediated proximal polyadenylation of sense and antisense transcription. In genotypes such as *fca-9*, where FCA is non-functional, or in

the presence of the transcriptional activator FRIGIDA, which antagonises proximal PA by FCA, FLD continues to be co-transcriptionally targeted, but fails to carry out its repressive function.

Discussion

In this work, we have elucidated how a transcription-coupled repression mechanism enables analogue regulation of transcriptional output, where the chromatin state is set up by alternative termination. The mechanistic details of how the 3' processing decisions are linked to histone demethylation and thus low transcription are outlined in the accompanying paper. We build on this using a computational model to reveal the overall mechanism, where the level of productive transcriptional activity set by such an analogue mechanism determines the level of transcriptional antagonism to Polycomb silencing. Consequently, while the targeting of Polycomb to *FLC* is a mechanistically parallel process to the co-transcriptional processing/demethylation and not a linear downstream outcome, the different levels of transcriptional activity set by the transcription coupled repression can dictate the rate of establishment of Polycomb silencing (Fig. 7). We validated the model by a variety of means, including gene expression, histone modification and FLC-Venus imaging time courses in the wild-type and in cases disrupted via a Polycomb mutation. Our model also resolves the apparent contradiction between the observed FLD targeting to a transcriptionally active *FLC* locus, and its role as a repressor.

Transcriptional antagonism to Polycomb silencing is fundamental to our understanding of the silencing mechanism. Importantly, similar concepts have been used to understand Polycomb silencing in the mammalian context (Klose et al., 2013), and this antagonism has also been validated in a mammalian system (Holoch et al., 2021). Polycomb targets that can be stably switched from repressed to activated upon transient Polycomb perturbation, tend to have higher intrinsic transcription. Transcriptional antagonism of a chromatin mediated silencing mechanism involving Polycomb response elements has also been demonstrated recently in Drosophila (Voortman et al., 2022). Here, in a plant context, this antagonism sets the timescale for the slow switch into the digital Polycomb silenced state, in an interlinked three-way association between chromatin, transcription and co-transcriptional processing (Graphical Abstract). Judging from the H3K27me3 profiles in the wild type and *clf-2* mutant, this switch in warm conditions appears to utilise a Polycomb nucleation and spreading mechanism, as it does in cold conditions. It is currently unknown precisely how this warm Polycomb nucleation is controlled without apparently using elements like VEL proteins that induce nucleation by Polycomb in cold conditions (Yang et al., 2017).

Importantly, our model predicts chromatin state and transcriptional bistability in the case of the *fca-1* (null) mutant (Fig. S4B), whereas for *fca-3* and L*er*, only the silenced is fully stable. As a result, if

silencing can be established in *fca-1* (independently of FCA), for example mediated by cold-specific PRC2 accessories in the case of cold-induced silencing, we predict that both silenced and active states can each be stably maintained. Hence, our conceptual framework also explains why cold-induced Polycomb silencing can be maintained in *fca* (or *fld*) mutants. The model predicts that these proteins are needed only for Polycomb silencing establishment during development, but not for its maintenance. In future work, it would be very interesting to specifically test this prediction by removing FCA and/or FLD at a later developmental stage after silencing is established.

The cause of the proximal polyadenylation on both *FLC* strands remains to be defined but is likely to involve stalling of the RNA Pol II complex. RNA Pol II stalling is now recognised as a major transcriptional control point, frequently associated with premature termination (Fong et al., 2022; Noe Gonzalez et al., 2021; Wagner et al., 2023). Antisense transcription at *FLC* induces the formation of an R-loop in the 3' region, (Xu et al., 2021), likely the consequence of negative supercoiling induced by an RNA Pol II stall. Techniques such as NET-seq should help to unravel the basis of its formation. FCA has been proposed to recognize the R-loop, which is stabilized by the homeodomain protein NDX, as a chromatin 'tangle' (Sun et al., 2013; Xu et al., 2021), and promote proximal polyadenylation through recruitment of the 3' processing factors. Anti-termination factors that prevent the use of early termination sites have been implicated in tuning transcriptional output from eukaryotic polymerases (Gregersen et al., 2019). In the case of *FLC*, the transcriptional activator FRIGIDA has recently been shown to function at least partly by antagonising FCA mediated proximal cleavage and polyadenylation of *FLC* sense transcription at specific stages of embryo development (Schon et al., 2021). The presence of active FRIGIDA promotes distal polyadenylation and prevents *FLC* silencing, further supporting the view that FCA mediated proximal termination is essential for repression. Interestingly, FRIGIDA expression outside of a specific developmental stage fails to activate *FLC* expression (Schon et al., 2021): this reinforces the view that once Polycomb epigenetic silencing has been established, reactivating transcription is difficult, with simple upregulation of an activator being insufficient to overcome robust digital silencing.

Overall, we have revealed the mechanism of co-transcriptional silencing at *FLC*, an essential precursor for slow switching into the Polycomb silenced state. These features are included in an animation to help explain these molecular feedbacks, and how this mechanism can lead to expression of *FLC* in one of two stable expression states (Movie 1). We anticipate these mechanisms will have broad relevance, with additional examples emerging over time (Chen et al., 2023). It is particularly intriguing that many elements of this pathway, such as FLD and FCA, are conserved transcriptional/splicing regulators, that likely have functions at many targets. Their core role in an integrated sense/anti-sense transcriptional circuitry likely singles out *FLC* as being acutely sensitive to their action.

Methods

Plant materials

All the plants were homozygous for the indicated genotype. Seeds were surface sterilized in 40 % v/v commercial bleach for 10 min and rinsed 4 times with sterile distilled water. Seeds were then sown on standard half-strength Murashige and Skoog (MS) medium (0.22% MS, 8% plant agar) media plates and kept at 4°C in darkness for 3 days before being transferred to long day photoperiod conditions (16 h of light, 8 h dark).

Plant growth (Imaging)

Seeds were surface-sterilized with 5% (v/v) sodium hypochlorite for 5 min, rinsed with sterile water 4x for 1 min and stratified at 4°C for 2 days in water and in the dark. Seeds were plated on MES buffered Murashige and Skoog (GM-MS) media, pH 5.8, containing respective antibiotics and grown on vertically oriented petri plates for 7 days in long-day conditions (16 h light/8 h dark, 22/20°C).

Imaging

Time course imaging of FLC-Venus protein levels in the epidermis of L*er*, *fca* allelic mutants, the *clf-2* mutant as well as the *fca-3 clf-2* mutant, was performed using a Leica confocal Stellaris 8 microscope with a 20x multi-immersion objective (0.75 NA). Root tips (2 cm) were cut off and immersed in 1.5 µg/mL Propidium Iodide (PI, Sigma–Aldrich, P4864) in 1x PBS before being imaged immediately. The OPSL 514 laser was used at 5% power with 514 nm excitation for FLC-Venus and PI. In photon counting mode, Venus was detected between 518-550 nm with the HyD SMD2 detector, PI was detected between ~600-650 nm. Images were acquired with a laser speed of 400 Hz, line accumulation of 6 (pixel dwell time of 2.43 µs), a Z-step size of 0.95 µm and a pinhole size of 1 AU. The same settings were used at all imaging time points to allow direct comparison between genotypes and time points. The representative images were projected using a single middle slice from the PI channel to show the cell outline, and 10 slices of FLC-Venus channel were maximum intensity projected. In standard image presentation, the dynamic range of the FLC-Venus channel was pushed from 0-255 to 2-11, in enhanced image presentation, the dynamic ranged was pushed from 2-7. In Supp Fig S5, the dynamic range of FLC-Venus channel was enhanced from 0-255 to 2-20 for all images.

RNA extraction and RT-qPCR

Total RNA was extracted as previously described (Box et al. 2011). Genomic DNA was digested with TURBO DNA-free (Ambion Turbo Dnase kit AM1907) according to manufacturer´s guidelines,

before reverse transcription (RT) was performed. The RT reactions were performed with SuperScript IV reverse transcriptase (ThermoFisher, 18090010) following the manufacturer´s instructions using gene-specific primers. Primers are listed in Supplemental Table S1. For RNA sequencing experiments, RNA was further purified with the Qiagen Rneasy miniprep kit (74106).

RNA sequencing

Library preparation and sequencing was performed by Lexogen GmbH. RNA integrity was assessed on a Fragment Analyzer System using the DNF-471 RNA Kit (15 nt) (Agilent). Sequencing-ready libraries were generated from 100ng of input RNA using a QuantSeq 3' mRNA-Seq Library Prep Kit REV for Illumina (015UG009V0271) following standard procedures. Indexed libraries were assessed for quality on a Fragment Analyzer device (Agilent), using the HS-DNA assay and quantified using a Qubit dsDNA HS assay (Thermo Fisher). A sequencing-ready pool of indexed libraries were sequenced on an Illumina NextSeq 2000 with a 100-cycle cartridge using the Custom Sequencing Primer (CSP) at Lexogen GmbH.

Bioinformatics analysis

Data analysis of RNAseq data was performed by Lexogen GmbH using their standard pipeline. Read Quality was assessed by FastQC and trimmed for quality and adapter content with cutadapt version 1.18 (Martin, 2011). Clean reads were mapped to the Arabidopsis reference genome (TAIR10) with STAR version 2.6.1a (Dobin et al., 2013). Raw reads have been deposited on Short Read Archive (SRA) under the reference PRJNA980626, and can be accessed at: PRJNA980626. To calculate proximal to distal count ratios, read ends were counted for each identified polyA cluster ((Schon et al., 2021), FLC_polyA_cluster_coords.txt). Proximal polyadenylation clusters are defined as termination sites within the first Exon and Intron of *FLC* while distal clusters are in close proximity to the canonical polyadenylation site. For each biological sample, ratios were calculated from the summed proximal and distal cluster counts (FLC_termination_clusters.txt).

ChIP timecourse for histone modifications

2.5 g of 7-, 14-, or 21-day-old seedlings were crosslinked in 1% formaldehyde and grinded to fine powder. Nuclei were extracted using Honda buffer as described previously in Sun et al. 2013. In all histone ChIP reactions, sonication, immunoprecipitation, DNA recovery and purification were performed as previously described in Wu et al. 2016. The antibodies used were anti-H3 (ab176842), anti-H3K27me3 (Merck 07-449 and ab192985), anti-H3K36me3 (ab9050), anti-H3K4me1 (ab8895).

All ChIP data were quantified by qPCR with primers listed in Table S1. Values were normalized to H3 and internal control to either STM or ACT7.

H3K27me3 ChIP in *clf* mutant

2.0 g of 14-day-old seedlings were crosslinked in 1% formaldehyde and grinded to fine powder. Nuclei were extracted using Honda buffer as described previously in Sun et al. 2013. In all histone ChIP reactions, sonication, immunoprecipitation, DNA recovery and purification were performed as previously described in Wu et al. 2016. The antibodies used were anti-H3 (ab176842), and anti-H3K27me3 (ab192985). All ChIP data were quantified by qPCR with primers listed in Table S1. Values were normalized to H3 and internal control *STM*.

FLD ChIP

2.5 g seedlings were crosslinked in 0.685 mg/mL of EGS [ethylene glycol bis(succinimidyl succinate)] and 1% formaldehyde and grinded to fine powder. Nuclei were extracted using Honda buffer as described for histone ChIP. Nuclei pellets were resuspended in 600 µl of RIPA buffer (1% NP-40, 0.5% Sodium Deoxycholate, 0.1 % SDS in PBS) and sonicated 5 times for 5 min (30s ON/ 30s OFF) at high mode in a Bioruptor Pico (Diagenode). IP were performed overnight at 4°C using 1.5 mg of pre-coated epoxy Epoxy Dynabeads (M-270) with 1.5 µl of anti-FLAG (Sigma, F1804) per reaction. Beads were then washed for 5 min twice with Low Salt Buffer (150 mM NaCl, 0.1% SDS, 1% Triton X-100, 2 mM EDTA, 20 mM Tris-HCl), twice with Hight Salt Buffer (500 mM NaCl, 0.1% SDS, 1% Triton X-100, 2 mM EDTA, 20 mM Tris-HCl), and twice with TE buffer (1 mM EDTA, 10 mM Tris-HCl). DNA recovery and purifications were performed as for Histone ChIP. Results in Fig. 6B were normalized to IGN5.

Computational model

For a detailed description of the computational model, its assumptions, implementation, and analysis of simulation output, see Supplementary Information. Additional experimental considerations for modelling are also presented in the Supplementary Information.

Figure Captions

Figure 1: (A) Schematic showing two possible modes of regulating population level expression – Analogue and Digital. **(B)** Schematic of combined digital and analogue regulation observed experimentally in *fca* mutants. **(C)** Schematic showing the transcription coupled repression mechanism at *FLC*. Activating H3K4me1 can be added during productive transcription (green dashed

arrow). The repression mechanism consists of proximal polyadenylation and termination of sense and antisense transcription mediated by the RNA binding protein FCA, which then enables removal of transcriptionally activating H3K4me1 across the locus by the putative histone demethylase FLD. The removal of H3K4me1 can inhibit co-transcriptional processing by preventing the addition of H3K36me3, and consequently promotes further proximal termination. Thus, a feedback loop (highlighted by the black dashed arrows) is formed, where the occurrence of proximal termination promotes further proximal termination. **(D)** Schematic of the mathematical model, for the transcription coupled repression mechanism depicted in (C). The schematic highlights the key processes and interactions captured by the mathematical model: sense and antisense transcription, co-transcriptional addition of H3K4me1 (green dashed arrows), FCA mediated proximal termination of transcription, FLD mediated removal of H3K4me1, and the promotion of proximal termination by low H3K4me1 coverage. Feedback is again highlighted by black dashed lines.

Figure 2: (A) qPCR data for *FLC* expression, showing repression of a transgenic wild-type *FLC* construct (*FLC-15*) in an FCA overexpression genotype (*35S::FCA*), in 14 day old seedlings, and the attenuation of this repression for an *FLC* transgenic construct where antisense transcription is disrupted (*TEX1*). Error bars represent mean +/- s.e.m. (n = 3 biological replicates). **(B)** Quantseq data for 7-day old seedlings (7 days after sowing), showing quantification of polyadenylated transcripts mapped to the *FLC* locus in the parental Landsberg (L*er*) genotype, the *fca* mutants, and a *clf* mutant.

Figure 3: (A) Schematic of the combined mathematical model incorporating silencing H3K27 methylation, PRC2 mediated read-write maintenance of these modifications, and mutual antagonism between H3K27me3 and transcription. **(B)** FCA effectiveness parameter values for the three genotypes. **(C)** Predicted frequency of distal transcription events (steady state average over 100 simulated loci) in an ON state, for the model of the transcription coupled repression mechanisms shown in Fig. 1D. Each simulated locus was started in an active state with full H3K4me1 coverage and allowed to equilibrate over a duration of 5 cell cycles. Averaging was performed over the duration of the following 10 cell cycles. **(D)** Model predicted fractional coverage of H3K4me1 in an ON state for the model shown in Fig. 1D, simulated as in (B). **(E-F)** Predicted transcriptional changes over time obtained by simulating the combined model. **(E)** Predicted changes in frequency of transcription events averaged over 100 simulated loci in the parental L*er* genotype, showing a rapid switch to OFF from an initial ON state with full H3K4me1 coverage. **(F)** Predicted changes in the fraction of ON copies in the *fca* mutants, computed from simulations of 100 copies over 20 cell cycles, started in a full H3K4me1 covered ON state. Fractions are shown at the starting timepoint (0), and at the end of 7, 14, and 21 days from the start. See Supplementary Information for the definition of ON and OFF states used in this analysis.

Figure 4: (A-C) Model predictions for the combined model. **(D-H)** Experimental validation of model predictions. Levels are averaged across the *FLC* locus in both predictions and experiments. In (D-H), error bars represent mean +/- s.e.m. (n = 3 biological replicates). **(A,D)** Changes over time in fractional coverage of H3K27me3 predicted by the model (A) and measured by ChIP-qPCR in the *fca* mutants (D). **(B,E)** Changes over time in fractional coverage of H3K4me1 predicted by the model (B) and measured by ChIP-qPCR in the *fca* mutants (E). In A and B, the values shown indicate averages over 100 simulated copies started in a full H3K4me1 covered ON state and simulated over 20 cell cycles. The fractional coverages are shown at the starting timepoint (0), and at the end of 7, 14, and 21 days from the start. **(C,F)** Model predictions (C) and experimental validation from Quantseq data (F) of proximal to distal termination ratio of sense transcription, in the *fca* mutants and *clf* mutant (7 day old seedlings). Model predicted ratios are normalised to the predicted ratio for L*er*. Model predicted ratios were computed at the 7 day timepoint (averaged over the last 0.25 days leading up to this timepoint) for all four genotypes (average over 100 simulated loci as in Fig. 3B,C). The model qualitatively captures the relative changes in the proximal to distal ratio between mutants. Note that absolute predictions of the ratios would require estimates of lifetimes for the proximal and distal polyadenylated forms in each mutant. **(G,H)** ChIP-qPCR time course measurements of H3K27me3 (G), and H3K4me1 (H) across the *FLC* locus in the parental L*er* genotype and *fca* mutants.

Figure 4 – Supplementary 4: (A) Histograms showing probability distribution of switch OFF times for an individual locus, for L*er* and *fca-3*. Histograms are generated by simulating 100 copies, started in a full H3K4me1 covered ON state, and simulated over 20 cell cycles (very few copies switch to OFF in *fca-1* within 20 cell cycles). **(B)** Model predicts that the locus is in a bistable regime in the *fca-1* mutant, with both ON state and OFF state stably maintained across several cell cycles. Plots show fraction of ON copies (left column) and H3K27me3 fractional coverage (right column) for 100 simulated loci started in an ON state (full H3K4me1 coverage) (top row) or started in an OFF state (full H3K27me3 coverage) (bottom row). Fractions are shown at the starting timepoint (0), and at the end of 5, 10, and 20 cell cycles from the start. During steady state maintenance of the OFF state, the cell cycle-averaged H3K27me3 stabilises at an intermediate level due to the periodic dilution by DNA replication and subsequent slow accumulation. **(C-D)** ChIP-qPCR time course measurements of H3K36me3 across the *FLC* locus in the parental L*er* genotype and the *fca* mutants. Error bars represent mean +/- s.e.m. (n = 3 biological replicates). (D) shows modification levels averaged across the locus.

Figure 5: (A) Schematic showing the rationale for examining the *clf* mutant. Transition from a Polycomb nucleated state to a spread state is prevented in a *clf* mutant. The lack of stability of a nucleated state allows switching back to a digital ON state. Green circles: active modifications (H3K4me1); red circles: repressive modifications (H3K27me3). Bottom panel: consequently, the reduction over time in the number of ON cells observed in the parental L*er* genotype is expected to be disrupted in the *clf* mutant. **(B)** Model predicted changes over time in the fraction of ON copies of *FLC*, computed from simulations of 100 copies over 20 cell cycles, started in a full H3K4me1 covered ON state. Fractions are shown at the starting timepoint (0), and at the end of 7, 14, and 21 days from the start. **(C)** Experimental validation of model predictions by time course measurement of *FLC* transcript levels by qPCR, in the parental L*er* genotype, the mutant *clf-2*, the mutants *fca-3* and *fca-1*, and the double mutant *fca-3 clf-2*. Error bars represent mean +/- s.e.m. (n = 3 biological replicates). **(D)** FLC-Venus time-course imaging in the different genetic backgrounds. Representative confocal images of FLC-Venus signal at three timepoints in the epidermis of the root meristem of the parental genotype Ler, the single mutants *clf-2*, and *fca-3*, and the double mutant *fca-3 clf-2*. Grey shows the cell wall dye propidium iodide; FLC-Venus intensity is indicated by colour maps for standard and enhanced images, respectively. The same settings were used for imaging of all time points. The same image presentation is used for standard and enhanced images. Brightness and contrast of FLC-Venus signal were increased to generate the enhanced images (Note different scale on colour maps). Yellow boxes in *clf-2* highlight ON cell files at DAS7/14. Scale bar, 50 μm. DAS stands for days after sowing. **(E)** The model can capture the changes between L*er* and *clf*, in the spatial profile of H3K27me3 across the *FLC* locus. Top panel: model predicted profiles of H3K27me3 coverage (see Supplementary Information for detailed description of simulation). Model predicted profile is steady-state average over 100 simulated loci, started in an active chromatin state with full H3K4me1 and equilibrated over a time duration of 10 cell cycles. Bottom panel: H3K27me3 profiles measured by ChIP-qPCR in 7-day old seedlings. Error bars represent mean +/- s.e.m. (n = 3 biological replicates).

Figure 5 - Supplementary 5: FLC-Venus time course replicates with additional genotypes

Additional representative images of FLC-Venus signal in Ler, *clf-2*, *fca-3*, *fca-3 clf-2* as well as an additional intermediate allele *fca-4* and the strong allele *fca-1* at three time points. FLC-Venus intensity is indicated by colour map; grey shows the cell wall. Scale bar, 50 μm. DAS stands for days after sowing.

Figure 6: (A) Changes over time in *FLC* expression in Col-0 seedlings, measured by time-course qPCR. Error bars represent mean +/- s.e.m. (n = 3 biological replicates**). (B)** Changes over time in FLD targeting to the *FLC* locus, measured by time-course ChIP-qPCR quantification of 3xFLAG-

FLD in seedlings (Col-0 background) (normalized to IGN5). Error bars represent mean +/- s.e.m. (n = 3 biological replicates).

Figure 7: Schematic showing how analogue and digital regulation can combine in the context of Polycomb mediated silencing.

Graphical Abstract: Schematic showing the general interplay between transcriptional activity, chromatin state, and co-transcriptional processing that controls the transcriptional state, and the specific aspects of this interplay that regulate transcription at the *FLC* locus.

References

Alamos, S., Reimer, A., Niyogi, K.K., and Garcia, H.G. (2021). Quantitative imaging of RNA polymerase II activity in plants reveals the single-cell basis of tissue-wide transcriptional dynamics. Nature Plants *7*, 1037-1049.

Angel, A., Song, J., Dean, C., and Howard, M. (2011). A Polycomb-based switch underlying quantitative epigenetic memory. Nature *476*, 105-108.

Antoniou-Kourounioti, R.L., Meschichi, A., Reeck, S., Berry, S., Menon, G., Zhao, Y., Fozard, J.A., Holmes, T.L., Wang, H., Hartley, M., *et al.* (2023). Integrating analog and digital modes of gene expression at *Arabidopsis FLC*. eLife *In Press*.

Baxter, C.L., Šviković, S., Sale, J.E., Dean, C., and Costa, S. (2021). The intersection of DNA replication with antisense 3′ RNA processing in *Arabidopsis FLC* chromatin silencing. Proceedings of the National Academy of Sciences *118*, e2107483118.

Berry, S., Dean, C., and Howard, M. (2017). Slow Chromatin Dynamics Allow Polycomb Target Genes to Filter Fluctuations in Transcription Factor Activity. Cell Syst *4*, 445-457 e448.

Berry, S., Hartley, M., Olsson, T.S., Dean, C., and Howard, M. (2015). Local chromatin environment of a Polycomb target gene instructs its own epigenetic inheritance. eLife *4*, e07205.

Chalamcharla, V.R., Folco, H.D., Dhakshnamoorthy, J., and Grewal, S.I. (2015). Conserved factor Dhp1/Rat1/Xrn2 triggers premature transcription termination and nucleates heterochromatin to promote gene silencing. Proceedings of the National Academy of Sciences *112*, 15548-15555.

Chen, W., Zhu, T., Shi, Y., Chen, Y., Li, W.J., Chan, R.J., Chen, D., Zhang, W., Yuan, Y.A., Wang, X., *et al.* (2023). An antisense intragenic lncRNA SEAIRa mediates transcriptional and epigenetic repression of SERRATE in Arabidopsis. Proceedings of the National Academy of Sciences *120*, e2216062120.

Csorba, T., Questa, J.I., Sun, Q., and Dean, C. (2014). Antisense *COOLAIR* mediates the coordinated switching of chromatin states at *FLC* during vernalization. Proc Natl Acad Sci U S A *111*, 16160-16165.

Dobin, A., Davis, C.A., Schlesinger, F., Drenkow, J., Zaleski, C., Jha, S., Batut, P., Chaisson, M., and Gingeras, T.R. (2013). STAR: ultrafast universal RNA-seq aligner. Bioinformatics *29*, 15-21.

Dodd, I.B., Micheelsen, M.A., Sneppen, K., and Thon, G. (2007). Theoretical analysis of epigenetic cell memory by nucleosome modification. Cell *129*, 813-822.

Fang, X., Wang, L., Ishikawa, R., Li, Y., Fiedler, M., Liu, F., Calder, G., Rowan, B., Weigel, D., Li, P., *et al*. (2019). Arabidopsis FLL2 promotes liquid-liquid phase separation of polyadenylation complexes. Nature *569*, 265-269.

Fang, X., Wu, Z., Raitskin, O., Webb, K., Voigt, P., Lu, T., Howard, M., and Dean, C. (2020). The 3' processing of antisense RNAs physically links to chromatin-based transcriptional control. Proc Natl Acad Sci U S A *117*, 15316-15321.

Fong, N., Sheridan, R.M., Ramachandran, S., and Bentley, D.L. (2022). The pausing zone and control of RNA polymerase II elongation by Spt5: Implications for the pause-release model. Molecular Cell *82*, 3632-3645.e3634.

Giorgetti, L., Siggers, T., Tiana, G., Caprara, G., Notarbartolo, S., Corona, T., Pasparakis, M., Milani, P., Bulyk, M.L., and Natoli, G. (2010). Noncooperative Interactions between Transcription Factors and Clustered DNA Binding Sites Enable Graded Transcriptional Responses to Environmental Inputs. Molecular Cell *37*, 418-428.

Goodrich, J., Puangsomlee, P., Martin, M., Long, D., Meyerowitz, E.M., and Coupland, G. (1997). A Polycomb-group gene regulates homeotic gene expression in Arabidopsis. Nature *386*, 44-51.

Gregersen, L.H., Mitter, R., Ugalde, A.P., Nojima, T., Proudfoot, N.J., Agami, R., Stewart, A., and Svejstrup, J.Q. (2019). SCAF4 and SCAF8, mRNA Anti-Terminator Proteins. Cell *177*, 1797-1813.e1718.

Holoch, D., Wassef, M., Lövkvist, C., Zielinski, D., Aflaki, S., Lombard, B., Héry, T., Loew, D., Howard, M., and Margueron, R. (2021). A cis-acting mechanism mediates transcriptional memory at Polycomb target genes in mammals. Nature Genetics *53*, 1686-1697.

Inagaki, S., Takahashi, M., Takashima, K., Oya, S., and Kakutani, T. (2021). Chromatin-based mechanisms to coordinate convergent overlapping transcription. Nat Plants *7*, 295-302.

Klose, R.J., Cooper, S., Farcas, A.M., Blackledge, N.P., and Brockdorff, N. (2013). Chromatin Sampling—An Emerging Perspective on Targeting Polycomb Repressor Proteins. PLOS Genetics *9*, e1003717.

Koornneef, M., Hanhart, C.J., and van der Veen, J.H. (1991). A genetic and physiological analysis of late flowering mutants in Arabidopsis thaliana. Mol Gen Genet *229*, 57-66.

Lammers, N.C., Galstyan, V., Reimer, A., Medin, S.A., Wiggins, C.H., and Garcia, H.G. (2020). Multimodal transcriptional control of pattern formation in embryonic development. Proceedings of the National Academy of Sciences *117*, 836-847.

Liu, F., Marquardt, S., Lister, C., Swiezewski, S., and Dean, C. (2010). Targeted 3' Processing of Antisense Transcripts Triggers *Arabidopsis FLC* Chromatin Silencing. Science *327*, 94-97.

Liu, F., Quesada, V., Crevillén, P., Bäurle, I., Swiezewski, S., and Dean, C. (2007). The Arabidopsis RNA-Binding Protein FCA Requires a Lysine-Specific Demethylase 1 Homolog to Downregulate FLC. Molecular Cell *28*, 398-407.

Lövkvist, C., and Howard, M. (2021). Using computational modelling to reveal mechanisms of epigenetic Polycomb control. Biochemical Society Transactions *49*, 71-77.

Mamrak, N.E., Alerasool, N., Griffith, D., Holehouse, A.S., Taipale, M., and Lionnet, T. (2022). The kinetic landscape of human transcription factors. bioRxiv, 2022.2006.2001.494187.

Marina, D.B., Shankar, S., Natarajan, P., Finn, K.J., and Madhani, H.D. (2013). A conserved ncRNA-binding protein recruits silencing factors to heterochromatin through an RNAi-independent mechanism. Genes & Development *27*, 1851-1856.

Marquardt, S., Raitskin, O., Wu, Z., Liu, F., Sun, Q., and Dean, C. (2014). Functional consequences of splicing of the antisense transcript COOLAIR on FLC transcription. Mol Cell *54*, 156-165.

Martignago, D., Bernardini, B., Polticelli, F., Salvi, D., Cona, A., Angelini, R., and Tavladoraki, P. (2019). The Four FAD-Dependent Histone Demethylases of Arabidopsis Are Differently Involved in the Control of Flowering Time. Frontiers in Plant Science *10*.

Martin, M. (2011). Cutadapt removes adapter sequences from high-throughput sequencing reads. 2011 *17*, 3.

Mateo-Bonmatí, E., Fang, X., Zhu, P., Maple, R., Fiedler, M., Passmore, L.A., and Dean, C. (2023). The CPSF phosphatase module links proximal polyadenylation to chromatin silencing. BioRxiv.

Menon, G., Schulten, A., Dean, C., and Howard, M. (2021). Digital paradigm for Polycomb epigenetic switching and memory. Current Opinion in Plant Biology *61*, 102012.

Moll, P., Ante, M., Seitz, A., and Reda, T. (2014). QuantSeq 3′ mRNA sequencing for RNA quantification. Nature Methods *11*, i-iii.

Ng, K.K., Yui, M.A., Mehta, A., Siu, S., Irwin, B., Pease, S., Hirose, S., Elowitz, M.B., Rothenberg, E.V., and Kueh, H.Y. (2018). A stochastic epigenetic switch controls the dynamics of T-cell lineage commitment. Elife *7*.

Nielsen, M., Menon, G., Zhao, Y., Mateo-Bonmatí, E., Wolff, P., Zhou, S., Howard, M., and Dean, C. (2023). Antisense transcription and PRC2 repression function in parallel during vernalization. In preparation.

Noe Gonzalez, M., Blears, D., and Svejstrup, J.Q. (2021). Causes and consequences of RNA polymerase II stalling during transcript elongation. Nature Reviews Molecular Cell Biology *22*, 3-21.

Nojima, T., and Proudfoot, N.J. (2022). Mechanisms of lncRNA biogenesis as revealed by nascent transcriptomics. Nature Reviews Molecular Cell Biology *23*, 389-406.

Pease, N.A., Nguyen, P.H.B., Woodworth, M.A., Ng, K.K.H., Irwin, B., Vaughan, J.C., and Kueh, H.Y. (2021). Tunable, division-independent control of gene activation timing by a polycomb switch. Cell Rep *34*, 108888.

Saxton, D.S., and Rine, J. (2022). Distinct silencer states generate epigenetic states of heterochromatin. Molecular Cell *82*, 3566-3579.e3565.

Schon, M., Baxter, C., Xu, C., Enugutti, B., Nodine, M.D., and Dean, C. (2021). Antagonistic activities of cotranscriptional regulators within an early developmental window set FLC expression level. Proc Natl Acad Sci U S A *118*.

Shimada, Y., Carl, S.H., Skribbe, M., Flury, V., Kuzdere, T., Kempf, G., and Bühler, M. (2021). An enhancer screen identifies new suppressors of small-RNA-mediated epigenetic gene silencing. PLOS Genetics *17*, e1009645.

Shu, J., Chen, C., Thapa, R.K., Bian, S., Nguyen, V., Yu, K., Yuan, Z.-C., Liu, J., Kohalmi, S.E., Li, C., *et al.* (2019). Genome-wide occupancy of histone H3K27 methyltransferases CURLY LEAF and SWINGER in Arabidopsis seedlings. Plant Direct *3*, e00100.

Simpson, G.G., Dijkwel, P.P., Quesada, V., Henderson, I., and Dean, C. (2003). FY Is an RNA 3′ End-Processing Factor that Interacts with FCA to Control the Arabidopsis Floral Transition. Cell *113*, 777-787.

Siwek, W., Tehrani, S.S.H., Mata, J.F., and Jansen, L.E.T. (2020). Activation of Clustered IFNγ Target Genes Drives Cohesin-Controlled Transcriptional Memory. Molecular Cell *80*, 396-409.e396.

Sonmez, C., Bäurle, I., Magusin, A., Dreos, R., Laubinger, S., Weigel, D., and Dean, C. (2011). RNA 3' processing functions of *Arabidopsis* FCA and FPA limit intergenic transcription. Proceedings of the National Academy of Sciences *108*, 8508-8513.

Sun, Q., Csorba, T., Skourti-Stathaki, K., Proudfoot, N.J., and Dean, C. (2013). R-Loop Stabilization Represses Antisense Transcription at the *Arabidopsis FLC* Locus. Science *340*, 619-621.

Swiezewski, S., Liu, F., Magusin, A., and Dean, C. (2009). Cold-induced silencing by long antisense transcripts of an Arabidopsis Polycomb target. Nature *462*, 799-802.

Tucker, J.F., Ohle, C., Schermann, G., Bendrin, K., Zhang, W., Fischer, T., and Zhang, K. (2016). A Novel Epigenetic Silencing Pathway Involving the Highly Conserved 5'-3' Exoribonuclease Dhp1/Rat1/Xrn2 in Schizosaccharomyces pombe. PLOS Genetics *12*, e1005873.

Vo, T.V., Dhakshnamoorthy, J., Larkin, M., Zofall, M., Thillainadesan, G., Balachandran, V., Holla, S., Wheeler, D., and Grewal, S.I.S. (2019). CPF Recruitment to Non-canonical Transcription Termination Sites Triggers Heterochromatin Assembly and Gene Silencing. Cell Reports *28*, 267-281.e265.

Voortman, L., Anderson, C., Urban, E., Yuan, L., Tran, S., Neuhaus-Follini, A., Derrick, J., Gregor, T., and Johnston, R.J. (2022). Temporally dynamic antagonism between transcription and chromatin compaction controls stochastic photoreceptor specification in flies. Developmental Cell *57*, 1817-1832.e1815.

Wagner, E.J., Tong, L., and Adelman, K. (2023). Integrator is a global promoter-proximal termination complex. Molecular Cell *83*, 416-427.

Wang, Z.W., Wu, Z., Raitskin, O., Sun, Q., and Dean, C. (2014). Antisense-mediated FLC transcriptional repression requires the P-TEFb transcription elongation factor. Proc Natl Acad Sci U S A *111*, 7468-7473.

Wittmann, S., Renner, M., Watts, B.R., Adams, O., Huseyin, M., Baejen, C., El Omari, K., Kilchert, C., Heo, D.-H., Kecman, T., *et al.* (2017). The conserved protein Seb1 drives transcription termination by binding RNA polymerase II and nascent RNA. Nature Communications *8*, 14861.

Wu, Z., Ietswaart, R., Liu, F., Yang, H., Howard, M., and Dean, C. (2016). Quantitative regulation of *FLC* via coordinated transcriptional initiation and elongation. Proc Natl Acad Sci U S A *113*, 218-223.

Xu, C., Wu, Z., Duan, H.C., Fang, X., Jia, G., and Dean, C. (2021). R-loop resolution promotes co-transcriptional chromatin silencing. Nat Commun *12*, 1790.

Yang, H., Berry, S., Olsson, T.S.G., Hartley, M., Howard, M., and Dean, C. (2017). Distinct phases of Polycomb silencing to hold epigenetic memory of cold in *Arabidopsis*. Science *357*, 1142-1145.

Zhao, Y., Zhu, P., Hepworth, J., Bloomer, R., Antoniou-Kourounioti, R.L., Doughty, J., Heckmann, A., Xu, C., Yang, H., and Dean, C. (2021). Natural temperature fluctuations promote *COOLAIR* regulation of *FLC*. Genes Dev *35*, 888-898.

Supplementary Information

Proximal termination generates a transcriptional state that determines the rate of establishment of Polycomb silencing

Govind Menon[1], Eduardo Mateo-Bonmati[2,5], Svenja Reeck[2], Robert Maple[2], Zhe Wu[3], Robert Ietswaart[4], Caroline Dean[2], Martin Howard[1]

[1]Department of Computational and Systems Biology, John Innes Centre, Norwich Research Park NR4 7UH, UK
[2]Department of Cell and Developmental Biology, John Innes Centre, Norwich Research Park NR4 7UH, UK
[3]Key Laboratory of Molecular Design for Plant Cell Factory of Guangdong Higher Education Institutes, Institute of Plant and Food Science, Department of Biology, School of Life Sciences, Southern University of Science and Technology, Shenzhen, China
[4]Harvard Medical School, Department of Genetics, 77 Avenue Louis Pasteur, Boston, MA 02115, USA
[5]Current address: Centro de Biotecnología y Genómica de Plantas, Universidad Politécnica de Madrid (UPM) – Instituto Nacional de Investigación y Tecnología Agraria y Alimentaria (INIA)/CSIC, 28223 Pozuelo de Alarcón, Madrid, Spain

Computational Model

We built a stochastic model describing the dynamics of the activating and repressive histone modifications of interest, across a single *FLC* locus. The model also describes transcription events at the locus – sense and antisense – as well as alternative polyadenylation during these transcription events.

Model features:

Activating and repressive histone modifications

The mathematical model describes the modification state of each H3 histone at the *FLC* locus, with the whole locus represented by an array of 30 nucleosomes, consistent with the approximately 6 kilobases extent of the locus (nucleosomal DNA + linker DNA spans approximately 200 bp). The modifications described are: (1) H3K4me1, an activating modification associated with gene bodies in Arabidopsis, and known to exhibit significant differences between active and silenced states of *FLC*; (2) the Polycomb-mediated repressive modification H3K27me3 as well as possible H3K27me2, H3K27me1 and me0 states. The model assumes mutual exclusivity of K4me and K27me on the same H3 tail in line with experimentally observed mutual exclusivity in mESCs (Shema et al., 2016; Voigt et al., 2012) (Kim et al., 2013; Schmitges et al., 2011). Evidence from mammalian and yeast studies indicate that H3K27me is added non-processively (McCabe et al., 2012; Soares et al., 2017). Therefore, the model assumes stepwise addition of these modifications.

Sense and Antisense transcription

The model describes sense and antisense transcription events at the locus. The frequency of these events (assumed to represent transcription initiation or transition to elongation) is determined by the coverage of repressive H3K27me3 across the locus. This is consistent with Polycomb (PRC1) binding to H3K27me3 and controlling accessibility to gene regulatory elements by mediating compaction (Blackledge and Klose, 2021), as well as other potential H3K27me3-mediated mechanisms, such as inhibition of RNA Pol II release from the Transcription Start Site (TSS) (Zhang et al., 2020), thus preventing transitions into an actively transcribing Pol II state (Brookes et al., 2012). Our data indicates that both sense and antisense transcription at *FLC* are silenced by Polycomb – both types of transcripts are present at higher levels in the absence of Polycomb silencing, as observed in genotypes containing the *FLC* activator FRIGIDA, and in loss of function mutants of FCA and FLD.

Co-transcriptional addition of activating modifications

Activating modification such as H3K4me and H3K36me in many contexts and across organisms are known to be added co-transcriptionally (Chan et al., 2022). The association of the H3K4 methyltransferase complex with elongating RNA Pol II and the addition of this modification during transcriptional elongation has been demonstrated in *S. cerevisiae* (Soares et al., 2017). In the case of Arabidopsis H3K4me1, a genome wide analysis of the localization patterns of H3K4me1, of RNA Pol II, and of the different H3K4 methyltransferases, indicates that the co-transcriptional addition of H3K4me1 over the gene body is mediated mainly by the methyltransferase ATXR7 (Oya et al., 2022). Consistent with this role, an *ATXR7* mutant has been shown to partially suppress *FLC* activation by the activator FRIGIDA (Tamada et al., 2009).

Alternative polyadenylation mediated by coverage of activating modifications

The model assumes that higher overall coverage of H3K4me1 across the locus promotes distal termination of transcription. This assumption is in line with a potential feedback mechanism where H3K4me1 enables binding of the H3K36me3 methyltransferase (SDG8) and consequent H3K36me3-mediated assembly of splicing factors (Leung et al., 2019) which facilitate co-transcriptional processing. Such a role for H3K4 methylation is also consistent with evidence in yeast (Soares et al., 2017) and mammalian cells (Wang et al., 2023), indicating a role in facilitating productive transcriptional elongation.

Proximal termination mediated removal of activating modifications

The model assumes proximal termination of both sense and antisense mediates removal of H3K4me1. This is in line with the potential function of FLD as a demethylase (Inagaki et al., 2021), and the fact that genetically, FLD relies on FCA-mediated proximal termination of

antisense (Liu et al., 2007). The removal of H3K4me1 resulting from proximal PA is assumed to take place uniformly across the whole locus, as the data we currently have does not allow us to observe the spatial details of this process.

Polycomb nucleation and spreading

The model describes nucleation of H3K27me by Polycomb in the *FLC* nucleation region, where Polycomb silencing is known to be nucleated during cold-induced chromatin silencing of *FLC*. Subsequent H3K27me3 spreading across the locus in this context is known to depend on the plant PRC2 methyltransferase CLF and on an active cell cycle, while nucleation does not depend on either. Experimental evidence from a genome-wide ChIP-seq study showing H3K27me3 patterns in a *clf* mutant (Shu et al., 2019) indicates that a similar mechanism is involved in the early developmental silencing of *FLC* – the *clf* mutant shows a clear H3K27me3 peak in the *FLC* nucleation region, while spreading is compromised. Consistent with this, in the wild-type, H3K27me3 is assumed to spread to the rest of the locus through interactions with the nucleation region, through read-write feedback interactions. The spreading is assumed to rely on an active cell cycle – in the model, this is achieved by having the interactions with the nucleation region stronger in S/G2 phases.

Looping interactions mediating Polycomb activity

Experimental evidence indicates the existence of a gene loop mediating an interaction between the 5' and 3' ends of *FLC* (Crevillen et al., 2013; Li et al., 2018), with the level of interaction potentially depending the transcriptional state of the locus (Li et al., 2018). Significantly, this looping interaction is present in the silenced *FLC* state in the reference genotype Col-0, and consistently, a secondary peak of H3K27me3 is observed in published ChIP-seq data in *clf* (Shu et al., 2019). Therefore, we capture this interaction in the model by allowing for stronger interactions with the nucleation region for a designated "looping region" within the gene body.

Productive transcription antagonises H3K27me

Experimental evidence from mammalian systems indicates that productive transcription can promote removal of H3K27me through histone exchange. In addition, the H3K27me demethylases have been shown to physically interact with and co-localise on chromatin with elongating RNA Pol II, in *Drosophila* (Smith et al., 2008) and more specifically at the *FLC* locus (Yang et al., 2016). Both features have been captured in previous models of Polycomb silencing (Berry et al., 2017), and they are also incorporated in the current model. These features allow the rate of H3K27me turnover across the locus to be determined by the frequency of transcription events. Our model also incorporates alternative PA of both sense

and antisense transcription, allowing proximal PA and termination of RNA Pol II. The model assumes that only distal PA and termination (i.e., productive transcription events) can remove H3K27me through the above mechanisms.

Mutual exclusivity of sense and antisense at the same locus

We previously found that distal antisense transcription and sense *FLC* transcription are mutually exclusive at individual *FLC* loci (Rosa et al., 2016). Consistent with this mutual exclusivity, we have observed an anticorrelation between the levels of distal antisense transcripts and sense transcripts in multiple contexts, including different chromatin states of the *FLC* locus (Ietswaart et al., 2017; Zhao et al., 2021). While this evidence demonstrates a mutual exclusivity between full length (distal) sense and antisense transcription events, we currently do not have data to determine whether the mutual exclusivity applies to proximally terminated transcription events. However, for simplicity, the model assumes mutual exclusivity for both types of transcription events. This is realised by having a refractory period after a sense (antisense) transcription event, during which antisense (sense) initiation is not allowed to occur. The model assumes equal refractory periods for sense and antisense transcription, as well as for distal and proximal termination.

Inheritance of modified histones during DNA replication

In line with recent evidence indicating that only H3-H4 tetramers carrying repressive modifications are reliably inherited across DNA replication (Escobar et al., 2021), the model assumes that H3 pairs corresponding to an individual nucleosome are inherited with probability half to a daughter strand, only if at least one of the H3 carries K27 methylation.

Additional considerations for the model

Absence of a role for the L*er* *Mutator*-like transposable element at *FLC*

The *FLC* allele in the L*er* accession is known to contain a *Mutator*-like transposable element (TE) in intron 1 that causes lower expression from this allele relative to *FLC* alleles in other accessions (Michaels et al., 2003). This lower expression results from RNAi-mediated chromatin silencing of the TE element (Liu et al., 2004). However, experimental evidence indicates that the intermediate *FLC* expression levels in *fca* mutants are unlikely to be mediated by the TE. The TE has been shown to act *in cis* (Michaels et al., 2003), as expression of an *FLC* allele from the Columbia-0 (Col-0) accession is unaffected in F1 plants generated by a L*er* to Col-0 cross, while the L*er* *FLC* allele expression is attenuated by the TE. In our case, the intermediate expression in *fca* mutants could be observed for both the endogenous *FLC* (L*er* *FLC* containing TE) and the transgenic Venus tagged *FLC* (Col-0

FLC sequence), arguing against a role for the *cis*-acting TE mechanism in generating intermediate transcription states.

Role for H3K36me3

The above model only considers the histone modifications H3K4me1 and H3K27me, and does not explicitly consider H3K36me3. The Arabidopsis H3K36 methyltransferase SDG8 is known to recognise H3K4me1, so H3K4me1 removal might be expected to affect H3K36 methylation. Interestingly, *FLC* upregulation in an *fca* mutant is rescued in an *sdg8 fca* double mutant (Fang et al., 2020), indicating that H3K36me3 may be essential to set up an active transcriptional state at *FLC*. This is consistent with our previous ChIP-qPCR data at *FLC,* showing high levels of H3K4me1 and H3K36me3 at the locus in a high transcriptional state and low levels of both these modifications in a low transcriptional state (Fang et al., 2020). Recent evidence from *Saccharomyces cerevisiae,* shows that H3K36me3 is required for the effective co-transcriptional splicing and recruitment of splicing factors (Leung et al., 2019). Based on this evidence, FLD-mediated removal of H3K4me1 may cause reduced H3K36 methylation, which in turn promotes further early transcription termination. For simplicity, the model omits the H3K36me3 step and assumes that H3K4me1 implicitly mediates this effect on termination.

Direct physical interaction between transcription coupled repression and Polycomb

FCA has been reported to interact directly with the Arabidopsis PRC2 methyltransferase CLF *in vivo* (Tian et al., 2019). However, we have found no evidence of this interaction in our FCA immunoprecipitation followed by mass spectrometry (IP-MS) data or other published CLF IP-MS data (Fang et al., 2019; Liang et al., 2015), and hence this interaction is not further considered in our model or other analyses.

Model implementation

Locus description: The whole locus represented by an array of 30 nucleosomes (60 H3 histones), consistent with the approximately 6 kilobase extent of the locus (nucleosomal DNA + linker DNA spans approximately 200 bp).

Mutually exclusive H3 modifications: Each H3 histone can be in one of five modification mutually exclusive states: {-1,0,1,2,3} representing H3K4me1, H3 unmodified on K4 and K27, H3K27me1, me2, and me3 respectively. This means addition of K27me can take place only in the absence of H3K4me1 and vice versa. All transitions are assumed to be non-processive: only transitions involving addition/removal of a single methyl group are allowed. The modification state of the locus is

representing by an array S representing the modification states of the 60 histones. Each entry S_i can take the values {-1,0,1,2,3}. The array S is used to store the current state of all 60 histones over the course of the simulation. Note that we do not describe H3K36me3 in the model, as the evidence indicates it is downstream of H3K4me1, as described above and in the main text.

Alternative termination of transcription: Each transcription event (sense or antisense) has a probability of being proximally terminated. This probability is determined by both the current H3K4me1 fractional coverage (whole locus) and the FCA effectiveness parameter, as follows:

$$P(\text{Proximal}) = \delta_{Proximal} + (p_0 + p_{FCA})(1 - P_{K4me1})(1 - \delta_{Proximal} - \mu_{Distal}).$$

The probability of distal termination is given by:

$$P(\text{Distal}) = 1 - P(\text{Proximal}).$$

Here p_{FCA} represents FCA effectiveness parameter and p_0 captures possible FCA independent proximal termination. $(p_0 + p_{FCA})$ is constrained to be less than or equal to 1. P_{K4me1} represents the fractional coverage of H3K4me1, $\delta_{Proximal}$ is a residual proximal termination probability (some proximal termination occurs even when $P_{K4me1} = 1$), and μ_{Distal} is a residual probability for distal termination (some distal termination occurs even when $p_{FCA} = 1$ or $P_{K4me1} = 0$).

Transcriptional antagonism of Polycomb: (1) Histone exchange: during each distally terminated transcription event, iterating over the histones (entries of array S), for each histone, we generate a pseudo-random number from a uniform distribution (0,1) and set both entries corresponding to the current nucleosome to 0 if the generated number is less than $p_{ex}/2$ (see Supplementary Table). (2) Co-transcriptional Demethylation: During each distally terminated transcription event, iterating over the entries of array S, for each histone, we generate a pseudo-random number from a uniform distribution (0,1) and reduce the methylation state by one if the current state is {1, 2, or 3} AND the generated number is less than p_{dem} (see Supplementary Table).

Transcription mediated effects on H3K4 methylation: (1) Co-transcriptional addition of H3K4me1: Each unmodified H3 histone has a fixed probability p_{K4me}^{Transc}, of being methylated during a productive (distally terminated) transcription event (not in case of proximal termination). (2) H3K4 demethylation by FLD: Each H3 histone carrying H3K4me1 has a fixed probability p_{dem}^{FLD} of losing this modification during a proximally terminated transcription event.

H3K4me1 dynamics: The background turnover rate (independent of proximal termination and FLD) of H3K4me1 is set so that overall turnover rates of H3K27me3 and H3K4me1 are in the ratio

3.128/0.959, as measured in HeLa cells by a SILAC technique in (Zee et al., 2010). The H3K4 methylation propensities (background and transcription mediated) are chosen to be significantly higher than the K27me3 propensities, consistent with faster H3K4 methylation seen in time course evidence from mammalian systems.

H3K27me3 dynamics: Values for methylation rate constants are mostly chosen as in . The overall rate β alone is adjusted from its value in (Berry 2017) to allow for a changed interaction paradigm – instead of just nearest neighbour interactions, the current model allows long ranged interactions between nucleosomes across the whole locus, with any nucleosome being able to interact with any other within the locus at some rate (see below). To account for nucleation, spreading and the looping interaction, the nucleosome array representing the whole locus is divided into three subsets: nucleation region (NR, nucleosomes 1 to 3, i.e., histones 1 to 6), looping region (LR, nucleosomes 20 to 22, i.e., histones 39 to 44), and body region (Body, remaining nucleosomes). The choice of nucleosomes 19 to 21 for the looping region is consistent with the observed secondary nucleation peak observed around 4kb downstream of the *FLC* TSS in published data for the *clf* mutant (Shu et al., 2019).

The methylation propensities at each histone i are computed as:

$$r_i^{\mathrm{me}} = \beta\left(\delta_{\mathrm{S_{i,0}}}(\gamma_{\mathrm{me0\text{-}1}} + \mathrm{k_{me0-1}E_i}) + \delta_{\mathrm{S_{i,1}}}(\gamma_{\mathrm{me1\text{-}2}} + \mathrm{k_{me1-2}E_i}) + \delta_{\mathrm{S_{i,2}}}(\gamma_{\mathrm{me2\text{-}3}} + \mathrm{k_{me2-3}E_i})\right)$$

where E_i represents the PRC2 read-write feedback contribution.

For nucleation region histones, the PRC2 read-write feedback mediated contribution to the H3K27 methylation propensity is computed as:

$$E_i = \xi_{NR}^{NR}\sum_{j\in NR}\left(\rho_{\mathrm{me2}}\delta_{S_j,2} + \delta_{S_j,3}\right) + \xi_{LR}^{NR}\sum_{j\in LR}\left(\rho_{\mathrm{me2}}\delta_{S_j,2} + \delta_{S_j,3}\right) + \xi_{Body}^{NR}\sum_{j\in Body}\left(\rho_{\mathrm{me2}}\delta_{S_j,2} + \delta_{S_j,3}\right),$$

where ρ_{me2} is the relative activation of PRC2 by H3K27me2 as compared to H3K27me3. For the looping region histones, the PRC2 read-write feedback mediated contribution to the H3K27 methylation propensity is computed as:

$$E_i = \xi_{NR}^{LR}\sum_{j\in NR}\left(\rho_{\mathrm{me2}}\delta_{S_j,2} + \delta_{S_j,3}\right) + \xi_{LR}^{LR}\sum_{j\in LR}\left(\rho_{\mathrm{me2}}\delta_{S_j,2} + \delta_{S_j,3}\right) + \xi_{Body}^{LR}\sum_{j\in Body}\left(\rho_{\mathrm{me2}}\delta_{S_j,2} + \delta_{S_j,3}\right).$$

For the remaining gene body histones, the PRC2 read-write feedback mediated contribution to the H3K27 methylation propensity is computed as:

$$E_i = \xi_{NR}^{Body} \sum_{j \in NR} \left(\rho_{\mathrm{me2}} \delta_{S_j,2} + \delta_{S_j,3}\right) + \xi_{LR}^{Body} \sum_{j \in LR} \left(\rho_{\mathrm{me2}} \delta_{S_j,2} + \delta_{S_j,3}\right) + \xi_{Body}^{Body} \sum_{j \in Body} \left(\rho_{\mathrm{me2}} \delta_{S_j,2} + \delta_{S_j,3}\right).$$

Here the parameters ξ are chosen so that interactions between nucleosomes within the nucleation and looping region histones produce the highest contribution to feedback methylation, followed by the contribution of NR and LR nucleosomes to methylation of other gene body nucleosomes. This is consistent with the PRC2 enzymatic machinery localising mainly to the nucleation region. Also consistent with this, we assume lower contributions from gene body histones to the methylation of NR and LR nucleosomes, and the lowest contribution from interactions between gene body histones. Hence, we set the above parameters as follows:

$\xi_{NR}^{NR} = \xi_{LR}^{NR} = \xi_{NR}^{LR} = \xi_{LR}^{LR} > \xi_{NR}^{Body} = \xi_{LR}^{Body} > \xi_{Body}^{NR} = \xi_{Body}^{LR} > \xi_{Body}^{Body}$.

Following (Berry et al., 2017), a background "noisy" removal of H3K27 methylation is also included in the model, represented by the rate constant γ_{dem}.

Dependence on an active cell cycle: To implement the dependence of H3K27me3 spreading on an active cell cycle (as observed experimentally in (Yang et al., 2017)), the total cell cycle duration is divided into two parts: G1 and S/G2/M, with replication of the locus occurring at the midpoint of S/G2/M. The duration of G1 is assumed to be approximately half the total duration of the cell-cycle. The four parameters corresponding to interactions between the NR/LR and the body region (ξ_{NR}^{Body}, ξ_{LR}^{Body}, ξ_{Body}^{NR}, ξ_{Body}^{LR}) are reduced by a factor of 10 during the part of the cell cycle corresponding to G1 phase.

Spreading mutant: For simulating the spreading mutant (*clf-2*), we lower the contributions from the NR and LR nucleosomes to methylation of gene body nucleosomes (i.e., lower ξ_{NR}^{Body} and ξ_{LR}^{Body}), as well as the contribution from the gene body nucleosomes to methylation of the NR and LR nucleosomes (i.e., lower ξ_{Body}^{NR} and ξ_{Body}^{LR}).

De novo addition of H3K27me3: In addition to the differences in PRC2 feedback mediated contributions, the nucleation region (first three nucleosomes) is assumed to have a significantly higher *de novo* contribution to the H3K27 methylation propensity (γ_{me} parameters), consistent with evidence for *de novo* PRC2 targeting to this region during early developmental silencing of *FLC* (Shu et al., 2019).

H3K27me3 fractional coverage measure: Our previous studies of *FLC* silencing indicate that nucleation region H3K27me3 alone can significantly repress transcription, with the body region H3K27me3 making a relatively smaller additional contribution to repression. This finding is different

to the assumptions of Berry et al., where both H3K27me2 and H3K27me3 could repress. Furthermore, nucleation of H3K27me3 in the cold is sufficient to switch the locus to a digitally OFF state, as seen by FLC Venus imaging in the roots (Lovkvist et al., 2021). Potentially different contributions of the nucleation and looping region H3K27me3 versus the body region H3K27me3 to the transcriptional repression are captured by allowing a higher contribution from these NR and LR nucleosomes when computing the overall fractional coverage of H3K27me3:

$$P_{K27me3} = \eta P_{K27me3}^{NR+LR} + (1-\eta) P_{K27me3}^{Body}$$

Here P_{K27me3}^{NR+LR} and P_{K27me3}^{Body} represent fractional coverage of H3K27me3 in the nucleation region/looping region and the rest of the locus, respectively, and $0 < \eta < 1$. The overall fractional coverage, P_{K27me3} computed above, is then used to determine the transcription propensity (see below).

Polycomb repression of transcription: H3K27me3 coverage across the locus is assumed to determine the "transcription initiation" frequency, where the frequency is assumed to be a piecewise linear function with a saturation threshold (similar to the model in (Berry 2017)). Note that this frequency can also represent the transition of initiated Pol II into the elongating phase. Nucleation region and looping region contributions to the fractional coverage are assumed to be higher than the rest of the locus (see above). H3K27me3 coverage also has the same effect on sense and antisense initiation frequency.

$$f = \alpha\left(f_{max} - \frac{P_{K27me3}}{P_T}(f_{max} - f_{min})\right) \text{ for } P_{K27me3} < P_T$$

and

$$f = \alpha f_{min} \text{ for } P_{K27me3} \geq P_T$$

We also allow for a slightly higher transcription frequency in the H3K27me3 nucleated state compared to a fully H3K27me3 spread state. This is consistent with our previous datasets, where *FLC* transcriptional output is observed to reduce further during the post-cold transition to a spread state following nucleation. To enable this behaviour, we set $\eta < P_T$ so that the full silencing threshold is not reached even with full coverage of H3K27me3 in the nucleation and looping regions (i.e., even with $P_{K27me3}^{NR+LR} = 1$).

Published evidence based on sequencing of nascent RNA as well as our own qPCR data (Wu et al., 2016) indicates lower frequency of antisense transcription compared to sense transcription. This difference between sense and antisense transcription is captured by using different values of α for sense and antisense initiation frequency. Note that H3K4me1 does not affect the initiation frequency.

Histone inheritance during DNA replication: For each individual simulation, the DNA replication times are fixed deterministically, assuming a cell cycle duration of 22h (Rahni and Birnbaum, 2019). At each DNA replication timepoint, the Gillespie Stochastic Simulation Algorithm (SSA) is interrupted. We then iterate over the entries of the array S, where for each nucleosome at the locus carrying at least one H3K27me, its modification state is set to 0, i.e., the pair of entries corresponding to the nucleosome is set to 0, with a probability of 0.5. We assume here random inheritance of intact H3-H4 nucleosomes, with equal probability to each daughter strand. For each nucleosome, this is done by generating a pseudo-random number from a uniform distribution (0,1) and setting the corresponding histone modification states to 0 if the generated number is less than 0.5. In contrast, for each nucleosome carrying no H3K27me, the modification state is always set to zero, i.e., no inheritance of nucleosomes carrying only H3K4me1.

Model parameter values: H3K27me

Parameter	Description	Value used in model	Details
N	Number of histones	60	
k_{me}	PRC2-mediated methylation rate (histone^{-1} s^{-1})	$8 \cdot 10^{-6}$	
$k_{\mathrm{me0\text{-}1}}$	PRC2-feedback mediated methylation rate (me0 to me1) (histone^{-1} s^{-1})	$9k_{\mathrm{me}}$	
$k_{\mathrm{me1\text{-}2}}$	PRC2-feedback mediated methylation rate (me1 to me2) (histone^{-1} s^{-1})	$6k_{\mathrm{me}}$	
$k_{\mathrm{me2\text{-}3}}$	PRC2-feedback mediated methylation rate (me2 to me3) (histone^{-1} s^{-1})	k_{me}	
$\gamma_{\mathrm{me2\text{-}3}}$	Noisy methylation rate (me2 to me3) (histone^{-1} s^{-1})	$k_{\mathrm{me}}/20$	
$\gamma_{\mathrm{me1\text{-}2}}$	Noisy methylation rate (me1 to me2) (histone^{-1} s^{-1})	$k_{\mathrm{me1\text{-}2}}/20$	
$\gamma_{\mathrm{me0\text{-}1}}$	Noisy methylation rate (me0 to me1) (histone^{-1} s^{-1})	$k_{\mathrm{me0\text{-}1}}/20$	

γ_{me2-3}^{NR}	De novo methylation rate (me2 to me3) in Nucleation region (histone^{-1} s^{-1})	0.35 $\gamma_{me2\text{-}3}$	
γ_{me1-2}^{NR}	De novo methylation rate (me1 to me2) in Nucleation region (histone^{-1} s^{-1})	0.35 $\gamma_{me1\text{-}2}$	
γ_{me0-1}^{NR}	De novo methylation rate (me0 to me1) in Nucleation region (histone^{-1} s^{-1})	0.35 $\gamma_{me0\text{-}1}$	
β	Relative local PRC2-activity	0.55	
ρ_{me2}	Relative activation of PRC2 by H3K27me2	0.1	
γ_{dem}	Noisy demethylation rate of H3K27 (histone^{-1} s^{-1})	$4 \cdot 10^{-7}$	

Model parameter values: Nucleosome interaction parameters for PRC2 read-write feedback

$\xi_{NR}^{NR}=\xi_{LR}^{NR}=\xi_{NR}^{LR}=\xi_{LR}^{LR}$	Interactions within nucleation and looping regions	1	
$\xi_{NR}^{Body}=\xi_{LR}^{Body}$	Nucleation and looping region contributions to methylation of gene body nucleosomes	0.5 (L*er*, *fca-3*, *fca-1*) 0.01 (*clf-2*)	
$\xi_{Body}^{NR}=\xi_{Body}^{LR}$	Gene body contributions to methylation of nucleation and looping region nucleosomes	0.2 (L*er*, *fca-3*, *fca-1*) 0.12 (*clf-2*)	
ξ_{Body}^{Body}	Interactions within gene body region	0.01	

Model parameter values: Transcription and PA site choice

α_{sense}	Trans-acting gene activation for sense transcription	1	
$\alpha_{antisense}$	Trans-acting gene activation for antisense transcription	0.2	
f_{min}	Minimum transcription initiation	$f_{max}/40$	

	rate (s^{-1})		
f_{max}	Maximum transcription initiation rate (s^{-1})	$0.531 \cdot 10^{-3}$	
P_T	H3K27me3 coverage threshold for full repression of transcription	$1/3$	
$\delta_{Proximal}$	Residual probability of proximal termination	0.05	
μ_{Distal}	Residual probability of Distal termination	0.05	
p_0	Parameter representing FCA independent proximal termination	0.8	
p_{FCA}	Parameter representing FCA mediated proximal termination	0.2 (L*er*, *clf-2*), 0.15 (*fca-3*), 0 (*fca-1*)	
η	Weight parameter for relative contribution of NR+LR H3K27me3 to transcriptional repression	0.25	

Model parameter values: Transcription effects on modifications

p_{dem}	Demethylation probability of H3K27me (histone^{-1} distal transcription^{-1})	$4 \cdot 10^{-3}$	
p_{ex}	Histone exchange probability (histone^{-1} distal transcription^{-1})	$1 \cdot 10^{-3}$	
p_{dem}^{FLD}	Demethylation probability of H3K4me1 (histone^{-1} proximal transcription^{-1})	0.5	
p_{K4me}^{Transc}	Methylation probability for unmodified H3K4 during a distally terminated transcription event	$100\frac{k_{me}}{f_{max}}$	Computed as 100 times the PRC2-mediated methylation rate k_{me} (histone^{-1} s^{-1}), then normalised by transcription frequency (s^{-1}) to obtain probability per histone per transcription event.

Simulations

Model simulations were carried out using the Gillespie exact SSA (Gillespie, 1977). Simulations were coded in C++ and compiled using Clang/LLVM (version 14.0.0). The Mersenne Twister 19937 algorithm (Matsumoto and Nishimura, 1998), implemented in the GNU Scientific Library (GSL version 2.7), was used to generate pseudorandom numbers for the Gillespie SSA. The simulation code can be accessed at:
https://github.com/gm1613/FLC_transcription_coupled_repression_model.git

Initial conditions

In all cases – both for the analog module in isolation and the full model, the initial state was set to full coverage of H3K4me1.

Analysis of simulation output

Average levels of fractional coverage of histone modifications and average frequency of different transcription events and termination site usage (sense distal, antisense distal, sense proximal, antisense proximal) were computed by averaging over 500 individual trajectories. Individual trajectories were started at random (uniformly distributed) times in the cell cycle to avoid having all trajectories synchronised. To quantify switching to the digital OFF state (which in the model can correspond either to a Polycomb nucleated state or a spread state), we have to define what qualifies as an OFF state. In our analysis we classify an OFF state as any state for which:

$$P_{K27me3} > \chi P_T$$

where the parameter χ is chosen so that $\chi P_T < \eta$, and all the other parameters/quantities are as defined above. This condition on χ ensures that an H3K27me3 build-up in the nucleation region (even if this modification is absent across the rest of the locus), can be sufficient to qualify as a digitally OFF state. In all simulation results shown , χ is set to 0.25.

Comparing simulation output to ChIP data

In Fig. 5E, we compare the model predicted H3K27me3 profiles at *FLC* in the L*er* parental genotype and the Polycomb spreading mutant *clf-2* to the ChIP-qPCR measured profiles in these genotypes. To do this we used an approach developed in (Wu et al., 2016) for comparing model predicted Pol II profiles to those measured by ChIP. In our case, this method generates a predicted H3K27me3 ChIP profile by combining the fully spatially resolved model predicted profile with the resolution limiting effects arising from the sonication generated fragment size distribution inherent in ChIP based measurements. Mathematically, this method involves a convolution of the full model predicted profile with the probability distribution of fragment sizes generated during the ChIP experiment. Here we use

the same fragment size distribution estimated in (Wu et al., 2016). The code used to carry out this analysis is also provided at:

https://github.com/gm1613/FLC_transcription_coupled_repression_model.git

Supplemental Table S1. Primer sets used in this work.

Purpose	Oligonucleotide name	Oligonucleotide sequences (5' → 3')	
		Forward primer (F)	Reverse primer (R)
Genotyping	clf-2	AGAGAAGCTCAAACAAGCCATCGA	TTAACCCGGACCCGCATTTGTTTCGG
	LB_clf-2	GTCGGCGTGCGGCTGGCGGCG	
RT	FLC spliced		TTTGTCCAGCAGGTGACATC
	FLC unspliced		CTTTGTAATCAAAGGTGGAGAGC
	UBC		TTGTGCCATTGAATTGAACCC
qPCR	FLC spliced	AGCCAAGAAGACCGAACTCA	TTTGTCCAGCAGGTGACATC
	FLC unspliced	CGCAATTTTCATAGCCCTTG	CTTTGTAATCAAAGGTGGAGAGC
	UBC	CTGCGACTCAGGGAATCTTCTAA	TTGTGCCATTGAATTGAACCC
ChIP	FLC_-2285	ATCCAGAAAAGGGCAAGGAG	CGAATCGATTGGGTGAATG
	FLC_-1788	GGATTGATGTGGGGCACTAT	AGTCATGGGTAGGGCATGTG
	FLC_-1555	TGGAGGGAACAACCTAATGC	TCATTGGACCAAACCAAACC
	FLC_-321	ACTATGTAGGCACGACTTTGGTAAC	TGCAGAAAGAACCTCCACTCTAC
	FLC_5	GCCCGACGAAGAAAAAGTAG	TCCTCAGGTTTGGGTTCAAG
	FLC_246	CGACAAGTCACCTTCTCCAAA	AGGGGGAACAAATGAAAACC
	FLC_473	GGCGGATCTCTTGTTGTTTC	CTTCTTCACGACATTGTTCTTCC
	FLC_741	CGTGCTCGATGTTGTTGAGT	TCCCGTAAGTGCATTGCATA
	FLC_1212	CCTTTTGCTGTACATAAACTGGTC	CCAAACTTCTTGATCCTTTTTACC
	FLC_1613	TTGACAATCCACAACCTCAATC	TCAATTTCCTAGAGGCACCAA

	FLC_2094	AGCCTTTTAGAACGTGGAACC	TCTTCCATAGAAGGAAGCGACT
	FLC_2523	AGTTTGGCTTCCTCATACTTATGG	CAATGAACCTTGAGGACAAGG
	FLC_3276	GGGGCTGCGTTTACATTTTA	GTGATAGCGCTGGCTTTGAT
	FLC_3699	TGAAATGTTACGAATACTAGCGTGT	GGATCAAAACTACTAGCTAACCCTTG
	FLC_4406	AGAACAACCGTGCTGCTTTT	TGTGTGCAAGCTCGTTAAGC
	FLC_5090	CCGGTTGTTGGACATAACTAGG	CCAAACCCAGACTTAACCAGAC
ChIP (continuation)	FLC_5599	TGGTTGTTATTTGGTGGTGTG	ATCTCCATCTCAGCTTCTGCTC
	FLC_5715	CCTGCTGGACAAATCTCCGA	GGATTTTGATTTCAACCGCCGA
	FLC_6013	CGTGTGAGAATTGCATCGAG	AAAAACGCGCAGAGAGAGAG
	FLC_6189	TCCTAAACGCGTATGGTTGG	CCTTCATGGATGACGGAACT
	FLC_6480	TCCAGACGCCATTGTCATTA	AGAGTGCATTTTAACACTGACGA
	FLC_6810	TTGTAAAGTCCGATGGAGACG	ACTCGGCGAGAAAGTTTGTG
	FLC_7091	CATCGCTGTGTTATGCGTTT	GGCAAGTGTCGCAGTAAACA
	STM (for H3K27me3 normalization)	GCCCATCATGACATCACATC	GGGAACTACTTTGTTGGTGGTG
	ACT_+122 (for H3K36me3 normalization)	CGTTTCGCTTTCCTTAGTGTTAGCT	AGCGAACGGATCTAGAGACTCACCTTG
	ACT+939 (for H3K4me1 normalization)	TGCCCCGAGAGCAGTGTTCC	TGGACTGAGCTTCATCACCAACG
	IGN5 (for FLD normalization)	CCCTTAAGCGGACATGGTT	AATGTCGGCCAATCTTCTTG

References

Berry, S., Dean, C., and Howard, M. (2017). Slow Chromatin Dynamics Allow Polycomb Target Genes to Filter Fluctuations in Transcription Factor Activity. Cell Syst *4*, 445-457 e448.

Blackledge, N.P., and Klose, R.J. (2021). The molecular principles of gene regulation by Polycomb repressive complexes. Nature Reviews Molecular Cell Biology *22*, 815-833.

Brookes, E., de Santiago, I., Hebenstreit, D., Morris, K.J., Carroll, T., Xie, S.Q., Stock, J.K., Heidemann, M., Eick, D., Nozaki, N., *et al.* (2012). Polycomb associates genome-wide with a specific RNA polymerase II variant, and regulates metabolic genes in ESCs. Cell Stem Cell *10*, 157-170.

Chan, J., Kumar, A., and Kono, H. (2022). RNAPII driven post-translational modifications of nucleosomal histones. Trends in Genetics *38*, 1076-1095.

Crevillen, P., Sonmez, C., Wu, Z., and Dean, C. (2013). A gene loop containing the floral repressor FLC is disrupted in the early phase of vernalization. The EMBO journal *32*, 140-148.

Escobar, T.M., Loyola, A., and Reinberg, D. (2021). Parental nucleosome segregation and the inheritance of cellular identity. Nature Reviews Genetics *22*, 379-392.

Fang, X., Wang, L., Ishikawa, R., Li, Y., Fiedler, M., Liu, F., Calder, G., Rowan, B., Weigel, D., Li, P., *et al.* (2019). Arabidopsis FLL2 promotes liquid-liquid phase separation of polyadenylation complexes. Nature *569*, 265-269.

Fang, X., Wu, Z., Raitskin, O., Webb, K., Voigt, P., Lu, T., Howard, M., and Dean, C. (2020). The 3' processing of antisense RNAs physically links to chromatin-based transcriptional control. Proc Natl Acad Sci U S A *117*, 15316-15321.

Gillespie, D.T. (1977). Exact stochastic simulation of coupled chemical reactions. The journal of physical chemistry *81*, 2340-2361.

Ietswaart, R., Rosa, S., Wu, Z., Dean, C., and Howard, M. (2017). Cell-Size-Dependent Transcription of *FLC* and Its Antisense Long Non-coding RNA *COOLAIR* Explain Cell-to-Cell Expression Variation. Cell Syst *4*, 622-635 e629.

Inagaki, S., Takahashi, M., Takashima, K., Oya, S., and Kakutani, T. (2021). Chromatin-based mechanisms to coordinate convergent overlapping transcription. Nat Plants *7*, 295-302.

Kim, D.-H., Tang, Z., Shimada, M., Fierz, B., Houck-Loomis, B., Bar-Dagen, M., Lee, S., Lee, S.-K., Muir, T.W., Roeder, R.G., *et al.* (2013). Histone H3K27 Trimethylation Inhibits H3 Binding and Function of SET1-Like H3K4 Methyltransferase Complexes. Molecular and Cellular Biology *33*, 4936-4946.

Leung, C.S., Douglass, S.M., Morselli, M., Obusan, M.B., Pavlyukov, M.S., Pellegrini, M., and Johnson, T.L. (2019). H3K36 Methylation and the Chromodomain Protein Eaf3 Are Required for Proper Cotranscriptional Spliceosome Assembly. Cell Reports *27*, 3760-3769.e3764.

Li, Z., Jiang, D., and He, Y. (2018). *FRIGIDA* establishes a local chromosomal environment for *FLOWERING LOCUS C* mRNA production. Nature Plants *4*, 836-846.

Liang, S.C., Hartwig, B., Perera, P., Mora-García, S., de Leau, E., Thornton, H., de Alves, F.L., Rapsilber, J., Yang, S., James, G.V., *et al.* (2015). Kicking against the PRCs – A Domesticated Transposase Antagonises Silencing Mediated by Polycomb Group Proteins and Is an Accessory Component of Polycomb Repressive Complex 2. PLOS Genetics *11*, e1005660.

Liu, F., Quesada, V., Crevillén, P., Bäurle, I., Swiezewski, S., and Dean, C. (2007). The Arabidopsis RNA-Binding Protein FCA Requires a Lysine-Specific Demethylase 1 Homolog to Downregulate FLC. Molecular Cell *28*, 398-407.

Liu, J., He, Y., Amasino, R., and Chen, X. (2004). siRNAs targeting an intronic transposon in the regulation of natural flowering behavior in Arabidopsis. Genes Dev *18*, 2873-2878.

Lovkvist, C., Mikulski, P., Reeck, S., Hartley, M., Dean, C., and Howard, M. (2021). Hybrid protein assembly-histone modification mechanism for PRC2-based epigenetic switching and memory. Elife *10*.

Matsumoto, M., and Nishimura, T. (1998). Mersenne twister: a 623-dimensionally equidistributed uniform pseudo-random number generator. ACM Trans. Model. Comput. Simul. *8*, 3–30.

McCabe, M.T., Graves, A.P., Ganji, G., Diaz, E., Halsey, W.S., Jiang, Y., Smitheman, K.N., Ott, H.M., Pappalardi, M.B., Allen, K.E., *et al.* (2012). Mutation of A677 in histone methyltransferase EZH2 in human B-cell lymphoma promotes hypertrimethylation of histone H3 on lysine 27 (H3K27). Proc Natl Acad Sci U S A *109*, 2989-2994.

Michaels, S.D., He, Y., Scortecci, K.C., and Amasino, R.M. (2003). Attenuation of FLOWERING LOCUS C activity as a mechanism for the evolution of summer-annual flowering behavior in Arabidopsis. Proc Natl Acad Sci U S A *100*, 10102-10107.

Oya, S., Takahashi, M., Takashima, K., Kakutani, T., and Inagaki, S. (2022). Transcription-coupled and epigenome-encoded mechanisms direct H3K4 methylation. Nature Communications *13*, 4521.

Rahni, R., and Birnbaum, K.D. (2019). Week-long imaging of cell divisions in the Arabidopsis root meristem. Plant Methods *15*, 30.

Rosa, S., Duncan, S., and Dean, C. (2016). Mutually exclusive sense–antisense transcription at *FLC* facilitates environmentally induced gene repression. Nature Communications *7*, 13031.

Schmitges, Frank W., Prusty, Archana B., Faty, M., Stützer, A., Lingaraju, Gondichatnahalli M., Aiwazian, J., Sack, R., Hess, D., Li, L., Zhou, S., *et al.* (2011). Histone Methylation by PRC2 Is Inhibited by Active Chromatin Marks. Molecular Cell *42*, 330-341.

Shema, E., Jones, D., Shoresh, N., Donohue, L., Ram, O., and Bernstein, B.E. (2016). Single-molecule decoding of combinatorially modified nucleosomes. Science *352*, 717-721.

Shu, J., Chen, C., Thapa, R.K., Bian, S., Nguyen, V., Yu, K., Yuan, Z.-C., Liu, J., Kohalmi, S.E., Li, C., *et al.* (2019). Genome-wide occupancy of histone H3K27 methyltransferases CURLY LEAF and SWINGER in Arabidopsis seedlings. Plant Direct *3*, e00100.

Smith, E.R., Lee, M.G., Winter, B., Droz, N.M., Eissenberg, J.C., Shiekhattar, R., and Shilatifard, A. (2008). *Drosophila* UTX Is a Histone H3 Lys27 Demethylase That Colocalizes with the Elongating Form of RNA Polymerase II. Molecular and Cellular Biology *28*, 1041-1046.

Soares, L.M., He, P.C., Chun, Y., Suh, H., Kim, T., and Buratowski, S. (2017). Determinants of Histone H3K4 Methylation Patterns. Molecular Cell *68*, 773-785.e776.

Tamada, Y., Yun, J.-Y., Woo, S.c., and Amasino, R.M. (2009). ARABIDOPSIS TRITHORAX-RELATED7 Is Required for Methylation of Lysine 4 of Histone H3 and for Transcriptional Activation of *FLOWERING LOCUS C* The Plant Cell *21*, 3257-3269.

Tian, Y., Zheng, H., Zhang, F., Wang, S., Ji, X., Xu, C., He, Y., and Ding, Y. (2019). PRC2 recruitment and H3K27me3 deposition at *FLC* require FCA binding of *COOLAIR*. Science Advances *5*, eaau7246.

Voigt, P., LeRoy, G., Drury, William J., III, Zee, Barry M., Son, J., Beck, David B., Young, Nicolas L., Garcia, Benjamin A., and Reinberg, D. (2012). Asymmetrically Modified Nucleosomes. Cell *151*, 181-193.

Wang, H., Fan, Z., Shliaha, P.V., Miele, M., Hendrickson, R.C., Jiang, X., and Helin, K. (2023). H3K4me3 regulates RNA polymerase II promoter-proximal pause-release. Nature *615*, 339-348.

Wu, Z., Ietswaart, R., Liu, F., Yang, H., Howard, M., and Dean, C. (2016). Quantitative regulation of *FLC* via coordinated transcriptional initiation and elongation. Proc Natl Acad Sci U S A *113*, 218-223.

Yang, H., Berry, S., Olsson, T.S.G., Hartley, M., Howard, M., and Dean, C. (2017). Distinct phases of Polycomb silencing to hold epigenetic memory of cold in *Arabidopsis*. Science *357*, 1142-1145.

Yang, H., Howard, M., and Dean, C. (2016). Physical coupling of activation and derepression activities to maintain an active transcriptional state at *FLC*. Proc Natl Acad Sci U S A *113*, 9369-9374.

Zee, B.M., Levin, R.S., Xu, B., LeRoy, G., Wingreen, N.S., and Garcia, B.A. (2010). In vivo residue-specific histone methylation dynamics. J Biol Chem *285*, 3341-3350.

Zhang, Y.-Z., Yuan, J., Zhang, L., Chen, C., Wang, Y., Zhang, G., Peng, L., Xie, S.-S., Jiang, J., Zhu, J.-K., *et al*. (2020). Coupling of H3K27me3 recognition with transcriptional repression through the BAH-PHD-CPL2 complex in Arabidopsis. Nature Communications *11*, 6212.

Zhao, Y., Zhu, P., Hepworth, J., Bloomer, R., Antoniou-Kourounioti, R.L., Doughty, J., Heckmann, A., Xu, C., Yang, H., and Dean, C. (2021). Natural temperature fluctuations promote *COOLAIR* regulation of *FLC*. Genes Dev *35*, 888-898.

Figure 1

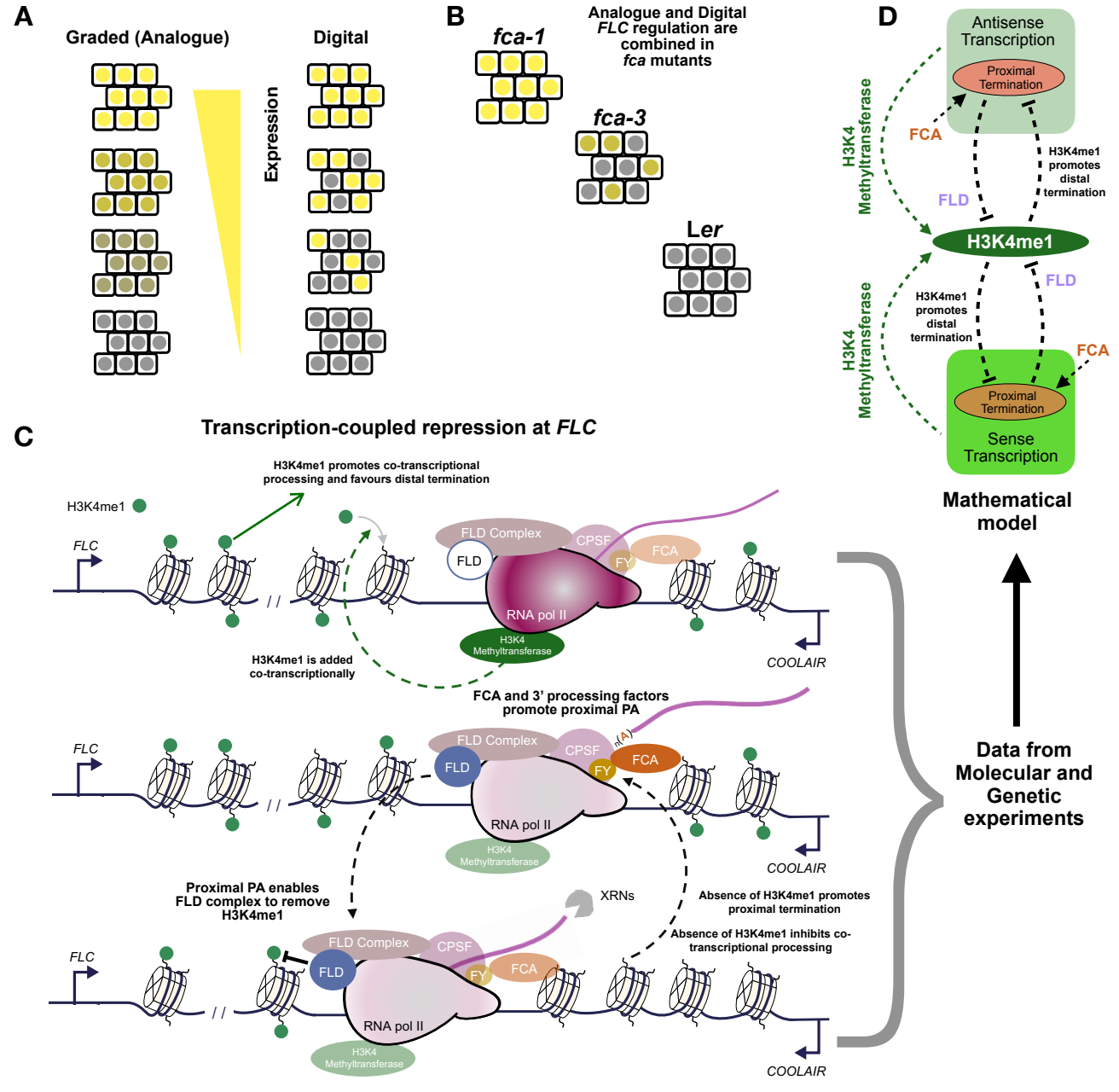
A
Graded (Analogue)
Digital
Expression
B
fca-1
fca-3
Ler
Analogue and Digital FLC regulation are combined in fca mutants
D
Antisense Transcription
Proximal Termination
FCA
FLD
H3K4 Methyltransferase
H3K4me1 promotes distal termination
H3K4me1
Sense Transcription
Mathematical model
Data from Molecular and Genetic experiments
C
Transcription-coupled repression at FLC
H3K4me1 promotes co-transcriptional processing and favours distal termination
H3K4me1
FLC
FLD Complex
FLD
CPSF
FY
FCA
RNA pol II
H3K4 Methyltransferase
COOLAIR
H3K4me1 is added co-transcriptionally
FCA and 3' processing factors promote proximal PA
n(A)
Proximal PA enables FLD complex to remove H3K4me1
XRNs
Absence of H3K4me1 promotes proximal termination
Absence of H3K4me1 inhibits co-transcriptional processing

Figure 2

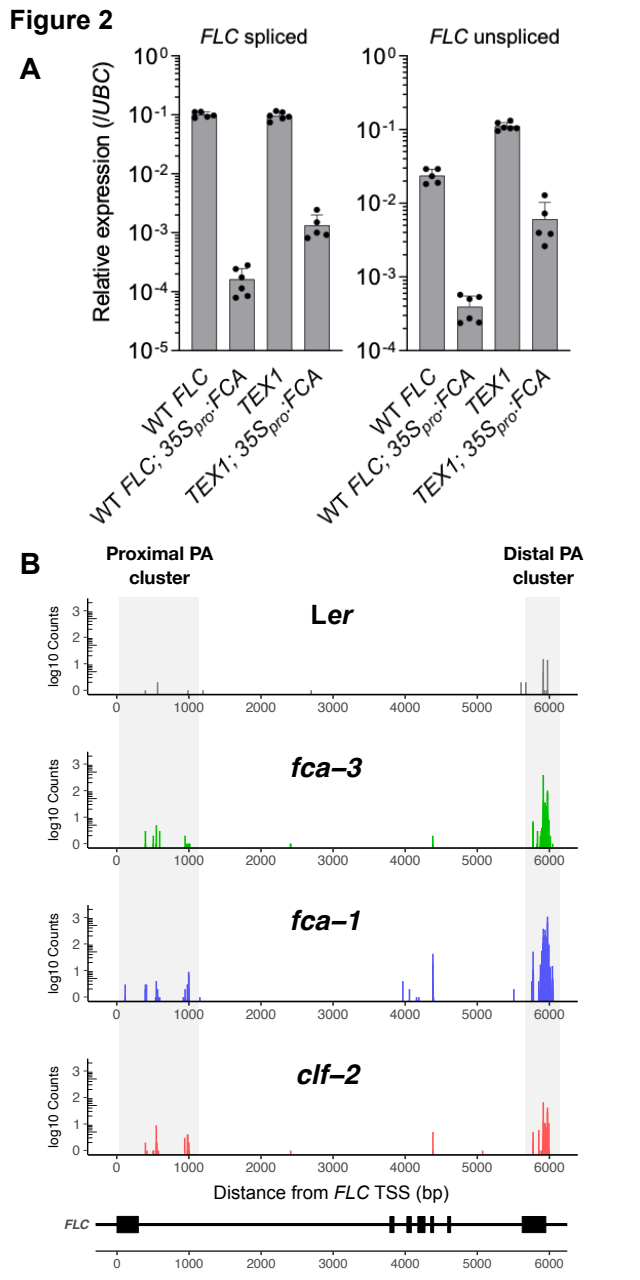
A
FLC spliced
FLC unspliced
Relative expression (/UBC)
WT FLC
WT FLC; 35Spro:FCA
TEX1
TEX1; 35Spro:FCA
B
Proximal PA cluster
Distal PA cluster
Ler
fca–3
fca–1
clf–2
log10 Counts
Distance from FLC TSS (bp)
FLC

Figure 3

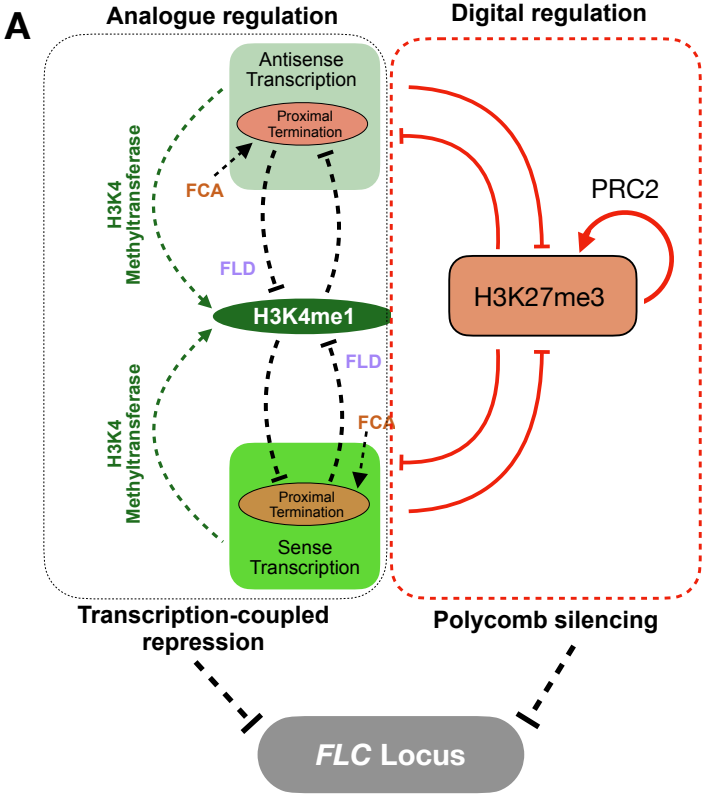
A
Analogue regulation
Digital regulation
Antisense Transcription
Proximal Termination
FCA
H3K4 Methyltransferase
FLD
H3K4me1
PRC2
H3K27me3
FLD
FCA
H3K4 Methyltransferase
Proximal Termination
Sense Transcription
Transcription-coupled repression
Polycomb silencing
FLC Locus

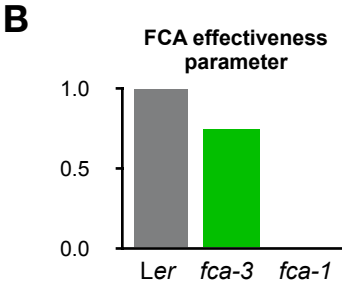
B
FCA effectiveness parameter
1.0
0.5
0.0
Ler
fca-3
fca-1

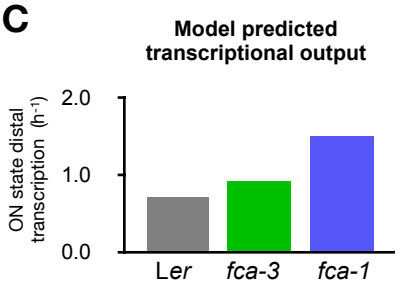
C
Model predicted transcriptional output
ON state distal transcription (h-1)
2.0
1.0
0.0
Ler
fca-3
fca-1

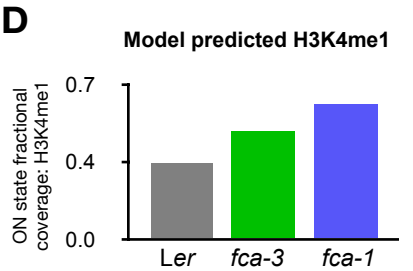
D
Model predicted H3K4me1
ON state fractional coverage: H3K4me1
0.7
0.4
0.0
Ler
fca-3
fca-1

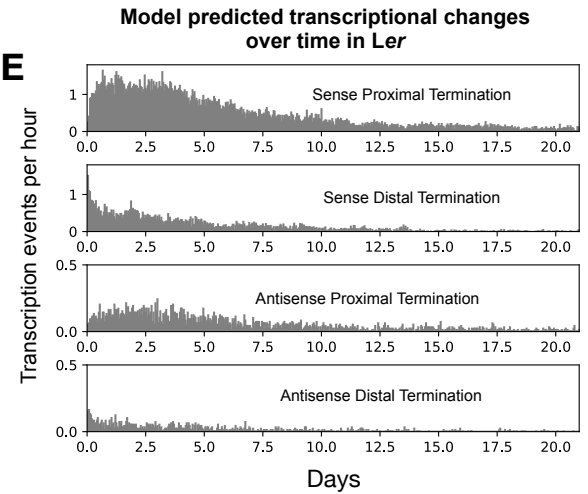
Model predicted transcriptional changes over time in Ler
E
Transcription events per hour
Sense Proximal Termination
Sense Distal Termination
Antisense Proximal Termination
Antisense Distal Termination
0.0
2.5
5.0
7.5
10.0
12.5
15.0
17.5
20.0
Days

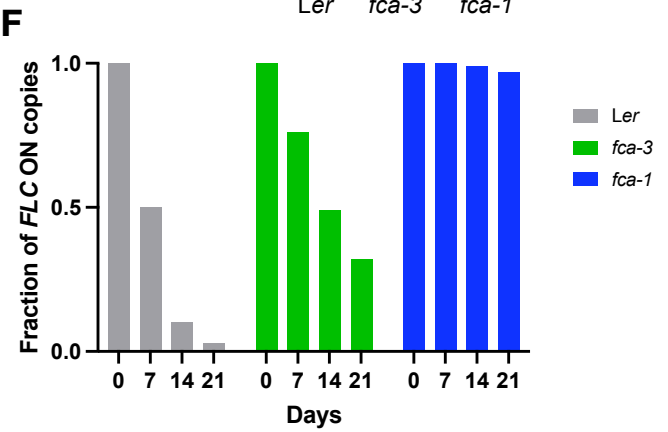
F
Fraction of FLC ON copies
1.0
0.5
0.0
0
7
14
21
Days
Ler
fca-3
fca-1

Figure 4

Model predictions

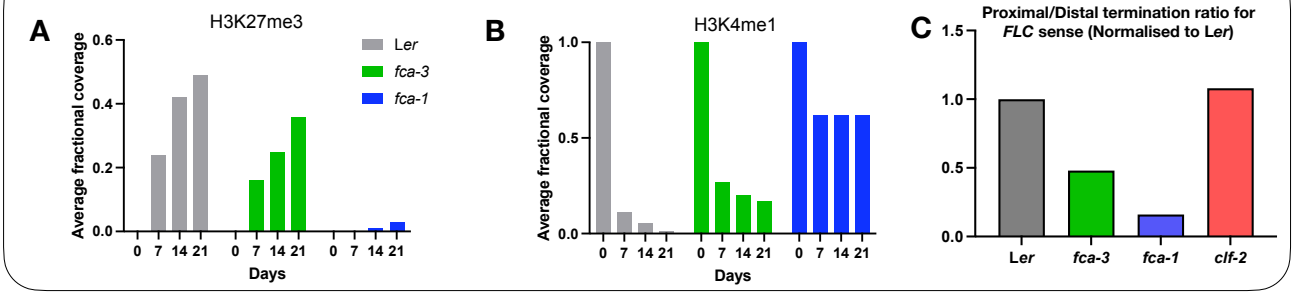

Experimental Validation

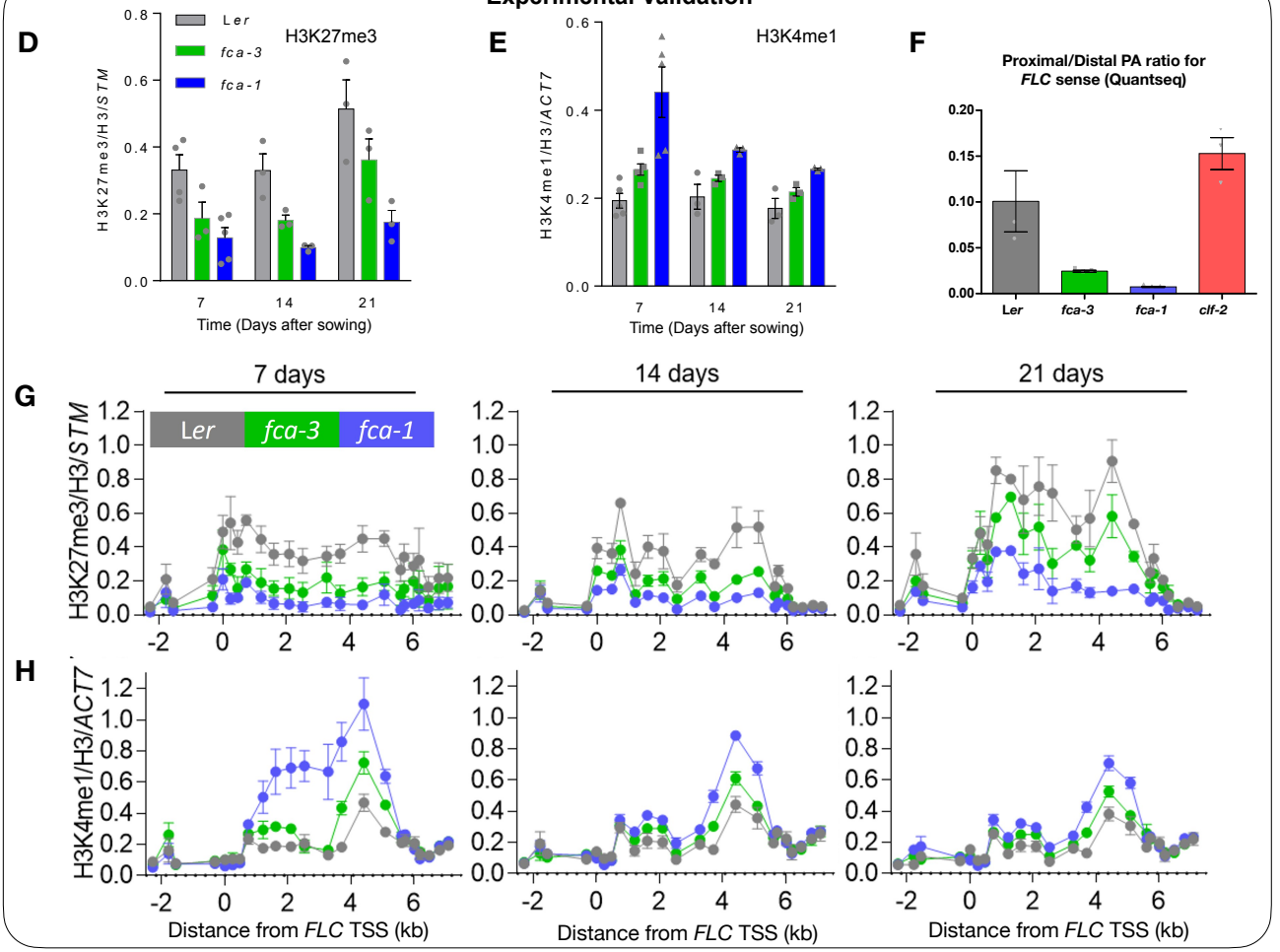

Figure S4

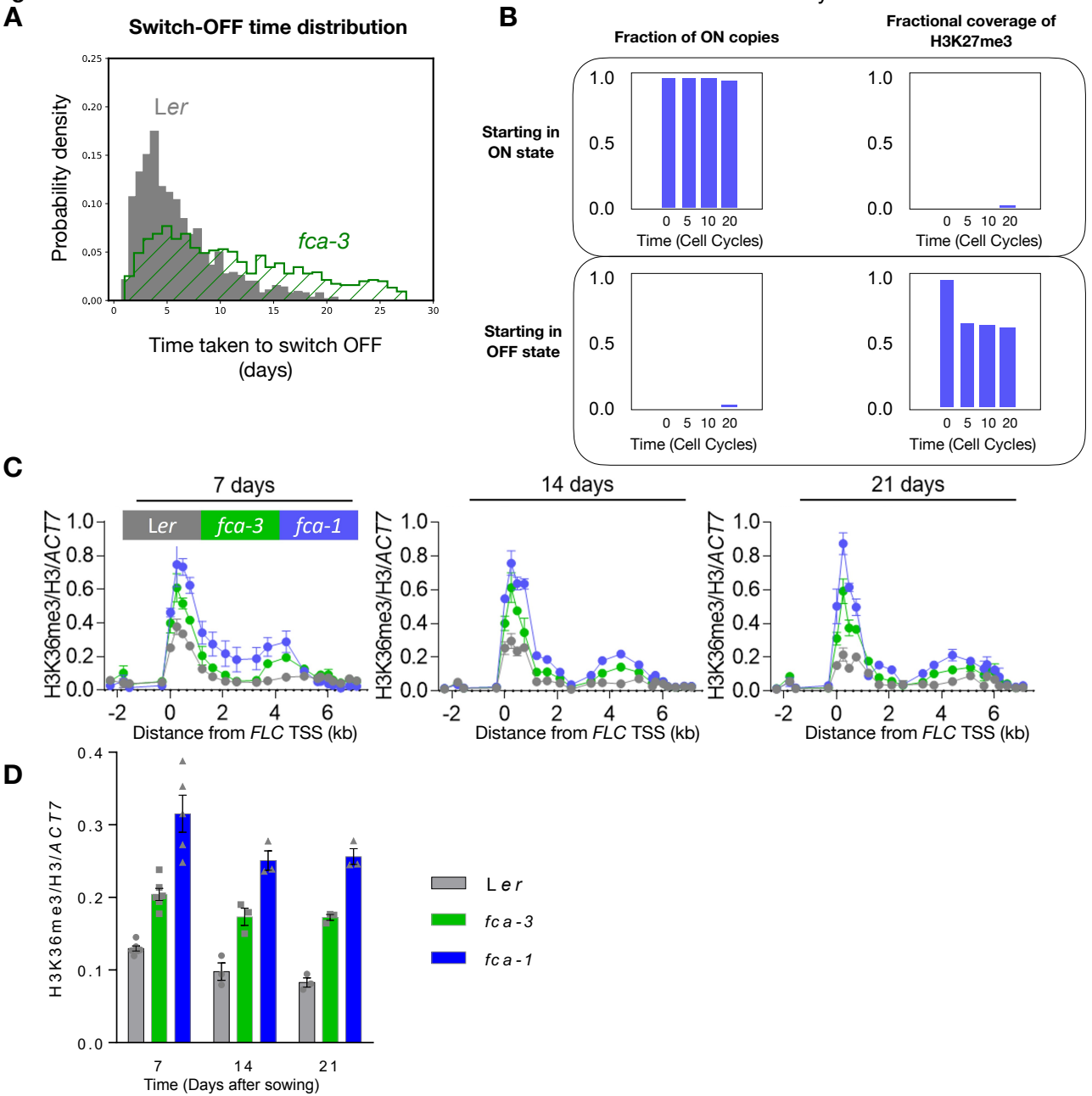
A
Switch-OFF time distribution
Probability density
Ler
fca-3
Time taken to switch OFF (days)
B
Bistability in fca-1
Fraction of ON copies
Fractional coverage of H3K27me3
Starting in ON state
Starting in OFF state
Time (Cell Cycles)
C
7 days
14 days
21 days
Ler
fca-3
fca-1
H3K36me3/H3/ACT7
Distance from FLC TSS (kb)
D
H3K36me3/H3/ACT7
Ler
fca-3
fca-1
Time (Days after sowing)

Figure 5

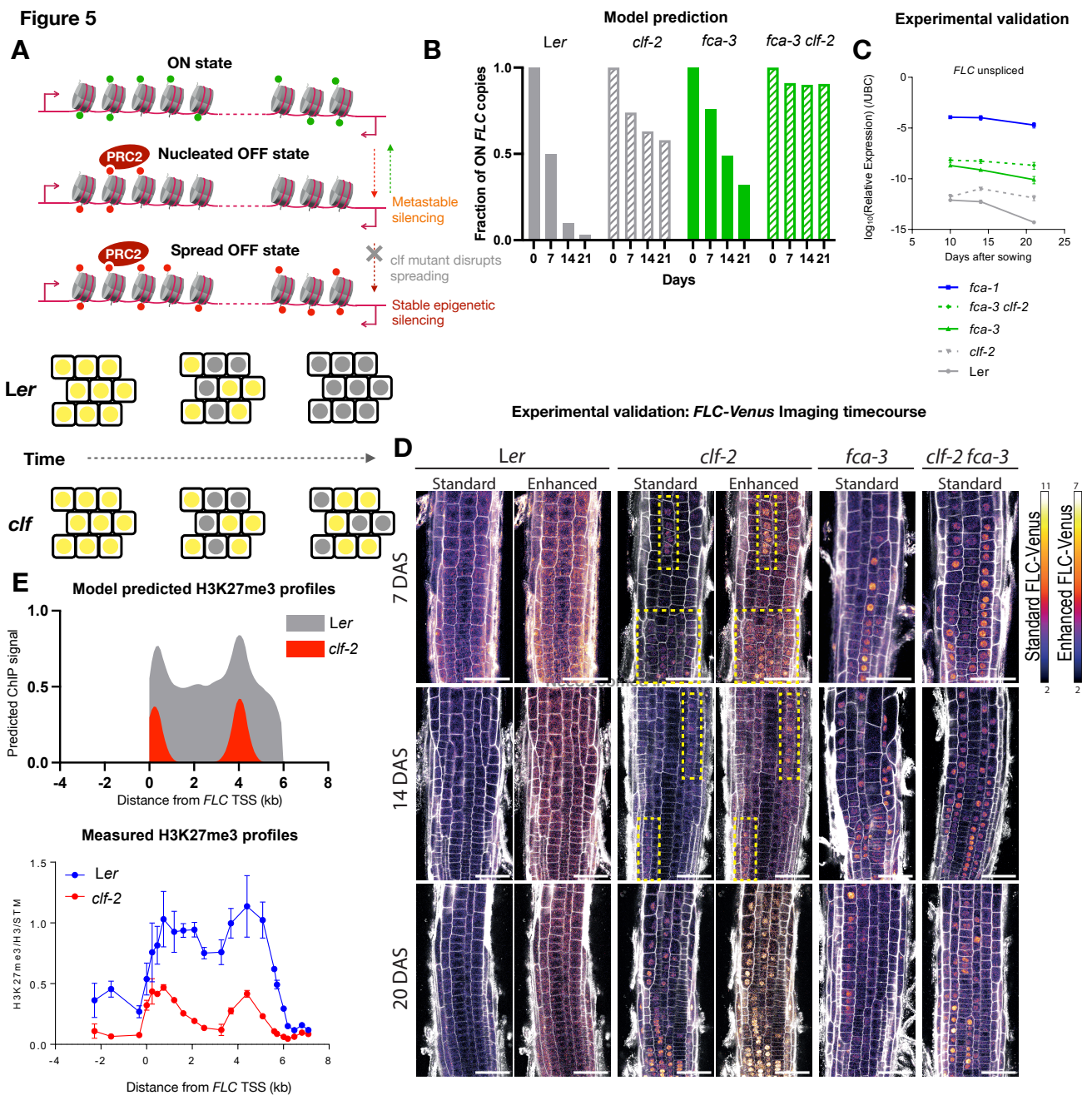
A
ON state
PRC2
Nucleated OFF state
Metastable silencing
PRC2
Spread OFF state
clf mutant disrupts spreading
Stable epigenetic silencing
Ler
Time
clf
B
Model prediction
Ler
clf-2
fca-3
fca-3 clf-2
Fraction of ON FLC copies
1.0
0.5
0.0
0 7 14 21
Days
C
Experimental validation
FLC unspliced
log10(Relative Expression) (/UBC)
0
-5
-10
-15
5 10 15 20 25
Days after sowing
fca-1
fca-3 clf-2
fca-3
clf-2
Ler
Experimental validation: FLC-Venus Imaging timecourse
D
Ler
clf-2
fca-3
clf-2 fca-3
Standard
Enhanced
7 DAS
14 DAS
20 DAS
Standard FLC-Venus
Enhanced FLC-Venus
11
2
7
2
E
Model predicted H3K27me3 profiles
Ler
clf-2
Predicted ChIP signal
1.0
0.5
0.0
-4 -2 0 2 4 6 8
Distance from FLC TSS (kb)
Measured H3K27me3 profiles
Ler
clf-2
H3K27me3/H3/STM
1.5
1.0
0.5
0.0
-4 -2 0 2 4 6 8
Distance from FLC TSS (kb)

Figure 6

A

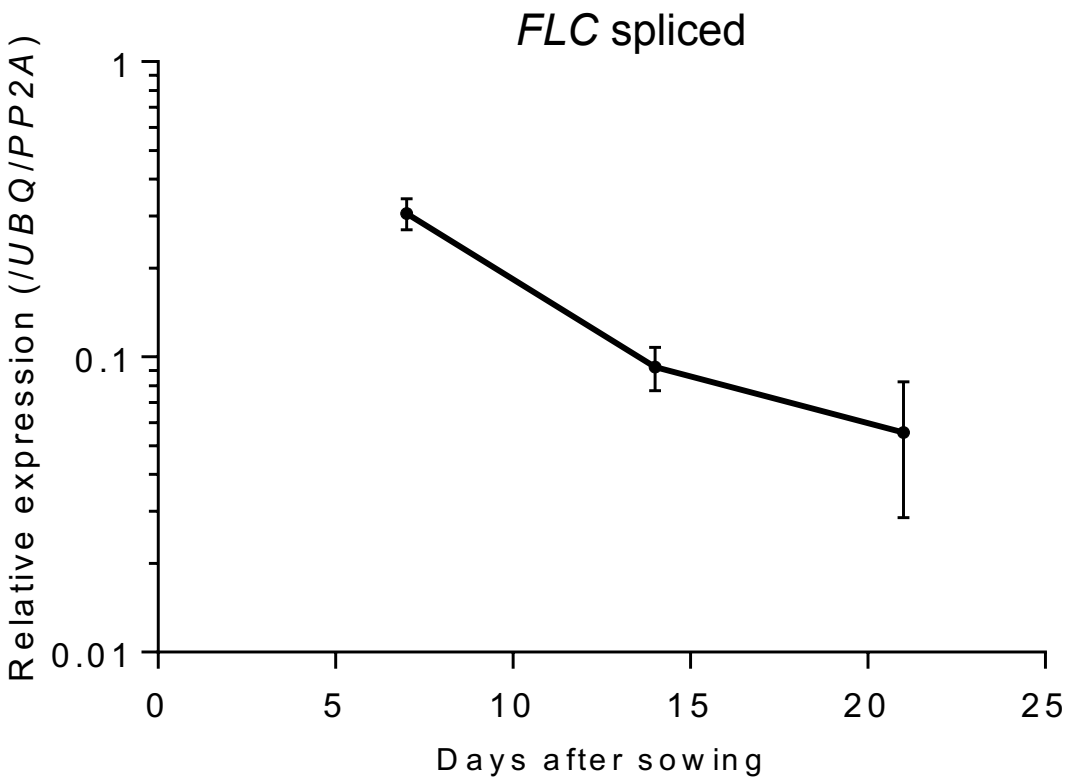
FLC spliced
Relative expression (*IUBQ/PP2A*)
1
0.1
0.01
0
5
10
15
20
25
Days after sowing

B

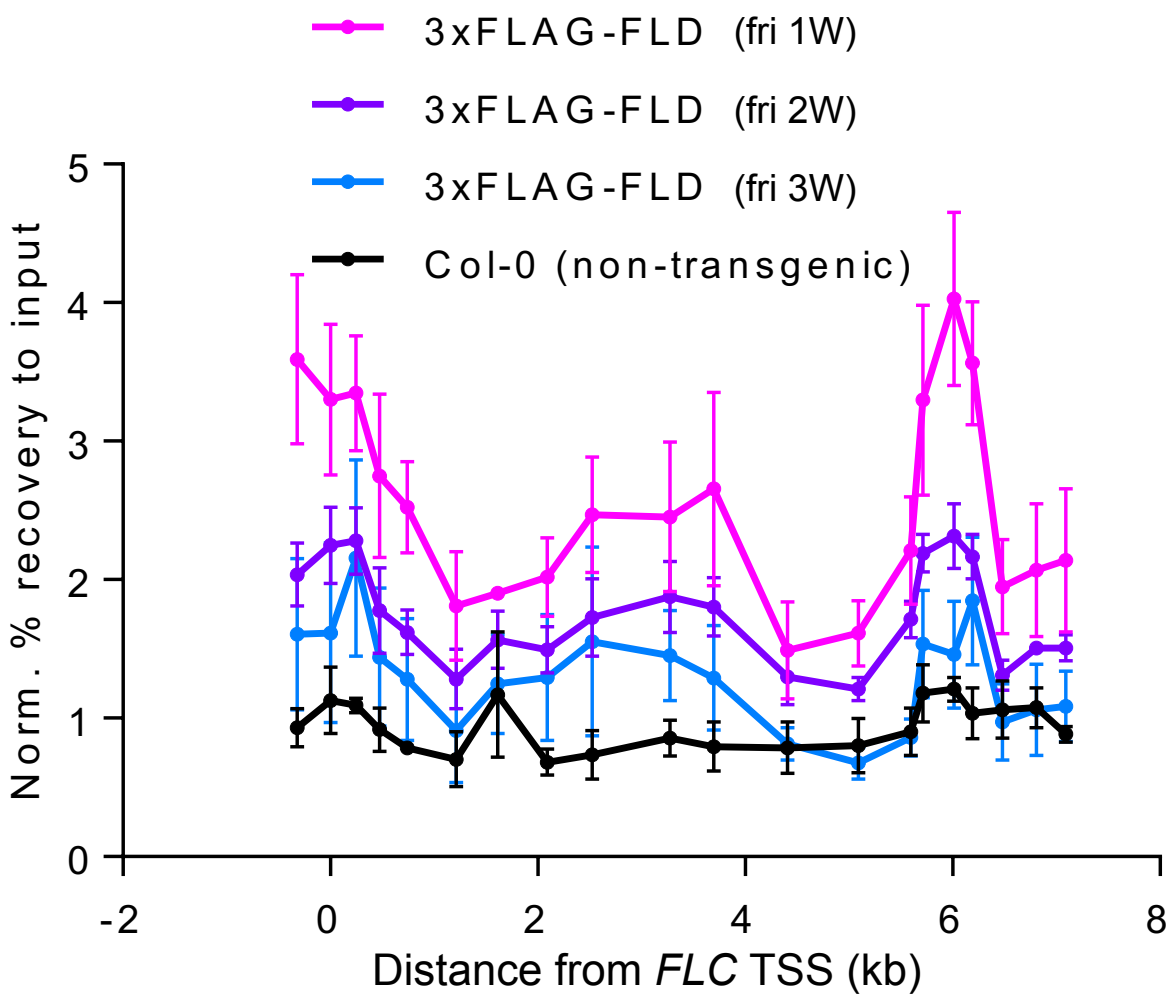
3xFLAG-FLD (fri 1W)
3xFLAG-FLD (fri 2W)
3xFLAG-FLD (fri 3W)
Col-0 (non-transgenic)
Norm. % recovery to input
5
4
3
2
1
0
-2
0
2
4
6
8
Distance from *FLC* TSS (kb)

Figure 7

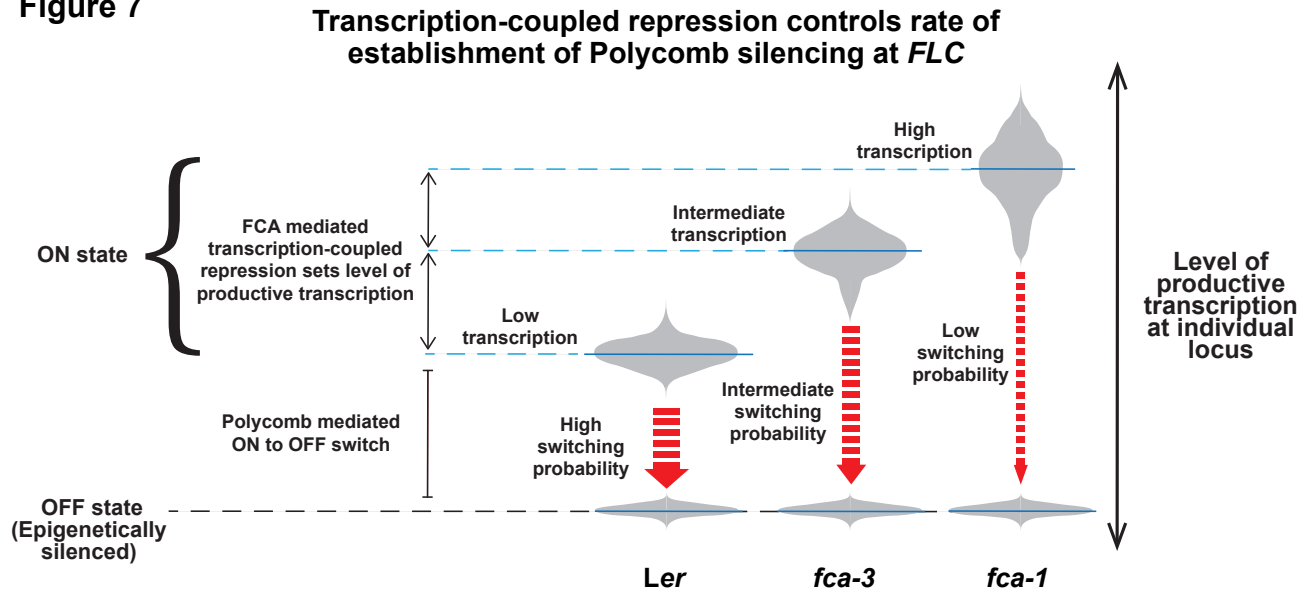
Transcription-coupled repression controls rate of establishment of Polycomb silencing at *FLC*
ON state
FCA mediated transcription-coupled repression sets level of productive transcription
Polycomb mediated ON to OFF switch
OFF state (Epigenetically silenced)
High transcription
Intermediate transcription
Low transcription
High switching probability
Intermediate switching probability
Low switching probability
Level of productive transcription at individual locus
Ler
fca-3
fca-1
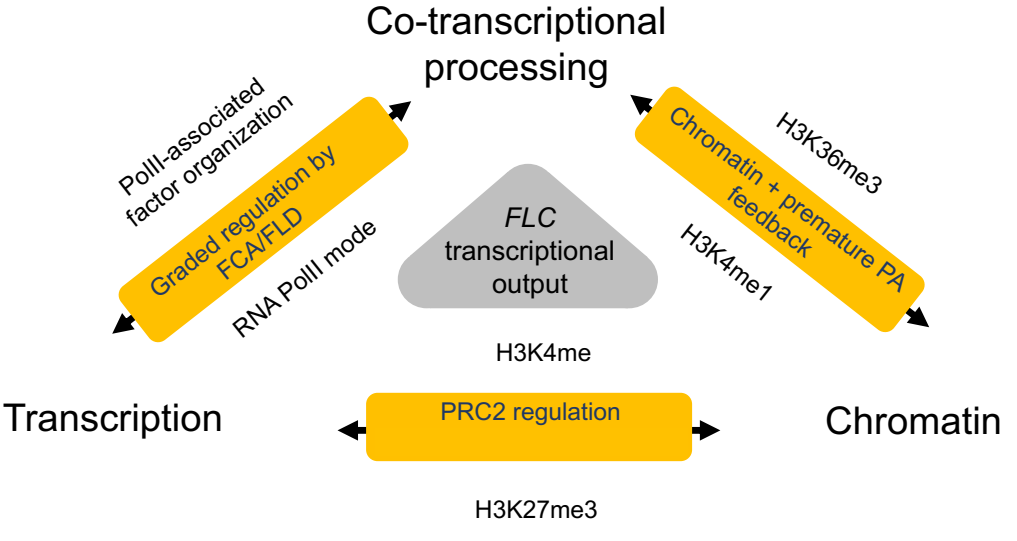
Graphical Abstract